Final Report

Enhancement of MF Performance via Membrane Stretching

By: Douglas Lloyd, Leah Worrel, Jason Morehouse

Department of Chemical Engineering
University of Texas at Austin
Austin, TX

Prepared for
National Water Research Institute
Fountain Valley, California

September 14, 2004

Table of Contents

EXECUTIVE SUMMARY

The hypothesis put forth in the proposal that lead to the funding of this project was that membrane *pore size characteristics* (maximum, minimum, and mean values of the major axis, minor axis, and aspect ratio) can be modified in a systematic fashion through uni-axial orientation. Furthermore, the proposal put forth the second hypothesis that *membrane performance* (flux, rejection, and permeate particle size distribution as a function of time) can be impacted by modifying the membrane pore size characteristics. The primary objective of the proposal originally funded by NWRI was to develop a fundamental understanding of the materials science of membrane stretching. In particular, the proposal called for determining how membrane material, initial membrane pore structure, and stretching conditions (rate and temperature) influenced the final membrane structure. Within the scope of the proposed primary objective was the development of a simulation package that would provide membrane manufacturers with a tool that could be used to tailor membranes via stretching. The secondary objective was to conduct permeation and particle challenge studies as a way of monitoring the impact of stretching on membrane performance. Implicit in the secondary object was the suggestion that it is possible to improve membrane performance for water treatment by controlling the characteristics of pores on the membrane surface. Ultimately, the goal was to test the hypotheses outlined above, to demonstrate feasibility, and to leverage NWRI money so that the project could continue beyond the end of NWRI funding. During the course of the project, the NWRI RAB restructured the project such that the stated secondary objective became the primary objective, and *vice versa.* Consequently, this documents reports progress towards each of the stated objectives; unfortunately, in the time frame of the research and in light of the redirection by the RAB, neither objective was fully met. However, progress was sufficient to allow the PI to leverage NWRI funds so that the project can continue.

Poly(ethylene teraphthalate) (PET) track-etched (T-E) membranes were supplied by Whatman, Inc. T-E membranes with nominal pores sizes ranging from 0.2 to 10 μm were stretched at temperatures between 80°C and 170°C with total strains up to 30%. A variety of poly(ether sulfone) and poly(vinylidene fluoride) phase inversion (PI/PS) membranes were supplied by Pall Corporation and Millipore Corporation. PI/PS membranes with nominal pore sizes ranging from 0.2 to 1.2 μm have been stretch at temperatures between 25°C and 160°C with total strains up to 150% and strain rates ranging from 0.1 to 6 cm/s. This report focuses on poly(ether sulfone) (PES) membranes of nominal pore size 0.2 μm supplied by Pall Corporation.

Surface pore size characteristics were measured using scanning electron micrographs and digital image analysis. Aspect ratio (length of major axis divides by length of minor axis) was shown to be a function of the amount of strain imposed on the membrane, although exactly how the aspect ratio – stain relationship depends on initial membrane pore characteristics, membrane material, strain rate, and stretching temperature has not been firmly established during this exploratory study. It was demonstrated that the pores in the PI/PS membranes change from a random orientation to uniform alignment as the amount of strain increases; however, again the exact way in which the pore alignment – stain relationship depends on initial membrane pore characteristics, membrane material, strain rate, and stretching temperature has not been firmly established during this exploratory study. The effects of stretching and annealing on the physical properties of the polymer were quantified using differential scanning calorimetry.

Permeation results for pure water feed as well as feed suspensions of irregular-shaped particulate mater and spherical beads and protein-containing feed solutions all showed that flux can be increased and flux declined decreased by stretching membranes. Membrane performance

did not increase by the same amount for every membrane studied and for each type of feed, which indicates that additional research is required to quantify the relationship between performance modification and membrane modification.

The research reported hear includes the initial steps towards the development of a mathematical model capable of relating final membrane structure to initial membrane structure, membrane material, and membrane stretching conditions. Although the development of this model was of a high priority in the proposal as originally funded by NWRI, it was subsequently de-emphasized as the RAB redirected the research. The modeling efforts are currently being continued under separate sponsorship.

NWRI funding allowed this project to proceed from a concept in the imagination of the PI to an active research project. As promised in the initial proposal, the NWRI funding provided the seed that allowed the PI to seek and successfully obtain additional from two other sources: The American Water Works Association Research Foundation and the Office of Naval Research.

ACKNOWLEDGEMENTS

This project was made possible through the generous financial support of NWRI and the Department of Chemical Engineering at The University of Texas at Austin. The research was completed by two PhD candidates, Leah S. Worrel and Jason A. Morehouse, under the supervision of Professor D.R. Lloyd. The following undergraduate students provided assistance in executing experiments and analysis: Dana Taylor, Cindy Smith, Ricky Villalobos, and Kristine McAndrews. In addition, valuable input was provided by Professor Desmond F. Lawler (UT, Civil Engineering), Professor Benny D. Freeman (UT, Chemical Engineering) and their students Leah Shimko and Bryan McCloskey.

The stretching device was generously donated by Gene Shipman of the 3M Company. Membrane samples were kindly provided by Tony Allegrezza (Millipore Corporation), Alex Chiang (Pall Corporation), and Dean Tsou (Whatman Inc.).

The NWRI Research Advisory Board appointed a sub-committee of Dave Furukawa, Bob Riley, and Bob Carnahan to oversee the project. Their input and suggestions were greatly appreciated.

The contributions of all of the people and organizations listed in the previous two paragraphs are gratefully acknowledged and sincerely appreciated.

INTRODUCTION

Microfiltration (MF) and ultrafiltration (UF) are widely used in water treatment facilities to remove macromolecules, particles, and colloids from water [1]. A major concern in these applications is the fouling of the membrane (that is, the irreversible blocking of pores by colloidal/particulate matter and by the macromolecules of natural organic matter). Numerous reports have been published on the deleterious effects fouling has on membrane performance (that is, flux and rejection) and the resulting additional cost of system operations [2-5]. The vast majority of these studies have focused on how the chemical and physical attributes of the foulant impact the extent of fouling. Only recently have publications appeared that shed some light on how fouling is impacted by the physical and chemical nature of the membrane [6-9]. Significant among the recent publications is a paper [10] for which the following results are relevant to the research proposed herein:

1. increased pore *aspect ratio* results in decreased surface attachment of both hydrophilic and hydrophobic bacterial strains, and
2. increased pore *aspect ratio* results in increased membrane flux,

where *aspect ratio* is defined as the ratio *major axis / minor axis*. The nine commercial membranes used in the previous study [10] had *average* aspect ratios ranging from 2 to 3, and each membrane had a spectrum of pores with different sizes and aspect ratios.

These findings were serendipitous in that the modest pore aspect ratio of the membranes studied resulted unintentionally from membrane formation procedures. The aspect ratio was not systematically controlled from membrane to membrane and showed a broad distribution within any given membrane. The findings resulted from thorough surface characterization of the membranes and multi-variable statistical analysis. The research reported here expands upon the earlier studies and provides fundamental knowledge that can serve as the basis for the design of microporous membranes of reduced particulate fouling and greater water flux.

To illustrate the impact of aspect ratio on fouling, consider the following argument. The onset of fouling occurs when a feed solution containing particles is introduced to an initially clean microporous membrane. A simplified picture of this event can be described in terms of a membrane with circular pores of diameter d and cross section $\pi d^2/4$. Flux of pure water through the membrane depends on d and the fraction of the membrane surface area comprised of pores. Figure 1 shows a pore of diameter d and the same pore after elongation. If a spherical particle of diameter D approaches a pore in such a way that the particle center of mass hits the membrane outside the perimeter of the pore, that particle does not influence subsequent transport through the pore. If the center of mass of the particle falls within the perimeter of the circular pore, it can either pass through the pore (if $D < d$) or be rejected by the pore (if $D > d$). If it is rejected, the particle will completely block the entrance to the pore and prevent subsequent liquid transport through that pore. While a particle of diameter $D < d$ passes through the circular pore, it is rejected by the elliptical pore. For the case of D slightly larger than d, the particle that completely blocks the circular pore only partially blocks the elliptical pore, thereby allowing water to continue permeation through a portion of the pore. This simple schematic diagram provides a starting point for investigation of the second observation of the previous study.

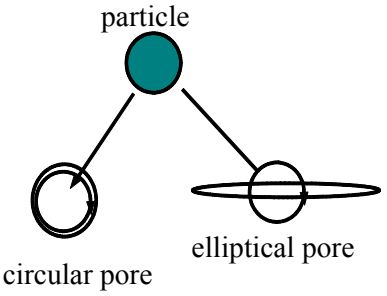

Figure 1: Particle approaching two pores of the same area.

PREVIOUS WORK

The process of stretching dense materials to form porous membranes is well known and documented [11, 12]. When one thinks of stretching films in association with membrane formation, one typically thinks of the Celgard® process in which pure polyolefin, such as high-density polyethylene (HDPE), is extruded under high stress to form a *dense film* referred to as a *precursor* [13]. This precursor is uniaxially stretched at room temperature, stretched again at an elevated temperature, and finally annealed. These thermal–mechanical steps are used to create pores, increase pore size, raise polymer crystallinity, and improve mechanical strength. In contrast to the Celgard process, which starts with a dense film, *this research focuses on the orientation of films that already contain distinct pores.* Track-etched (T-E) membranes are widely used for separations in which one needs a clear distinction between what size of particle passes through the membrane and what is rejected by the membrane. These membranes are advertised as having circular pore entrances and straight-through cylindrical pores with a rather narrow or uniform pore size distribution [14]; however, this study proves that these claims are only approximately true. The manufacture of T-E membranes is complex, so it has proven difficult to tailor pore sizes to anything other than the sizes currently available in commercial membranes. To our knowledge, there is no literature related to the stretching of T-E membranes and the impact on membrane performance. Most commercially available microporous membranes are made via phase inversion or phase separation processes (PI/PS). PI/PS membranes can either be anisotropic or isotropic in structure (where anisotropic indicates a pore size gradation in the direction of transport, and isotropic indicates no pore size gradation). PI/PS membranes typically have a cellular structure, thereby presenting a tortuous path through the membrane. They also have a pore size distribution somewhat larger than that found in T-E membranes. The process for making these membranes is well documented in the literature; consequently, no discussion of their formation is presented here other than to say that intentional orientation of the membrane is not typically a part of the membrane formation process. Membrane pore openings tend to be slightly elliptical, with aspect ratios ranging from 1.2 – 1.6 due to the manufacturing process. Our preliminary studies characterizing commercial MF and UF membranes indicate that aspect ratios are typically in the range 1 to 3.

As the following paragraphs illustrate, some recent work on the intentional stretching of microporous phase separation membranes has been reported in the patent literature. Researchers at 3M have done considerable work on stretching microporous films. For example, Shipman formed films from polyethylene (PE) in a low molecular weight *diluent* (60 wt-% PE) [15]. The films were then oriented in at least one direction after phase separation but prior to diluent extraction and subsequently annealed. Kinzer [16, 17] extrapolated Shipman's work by biaxially orienting cellular PE films. In this case, the films were stretched and heat set after diluent extraction. Diluent extraction and extractant evaporation processes were carried out on restrained films. Mrozinski [18-20] added the use of a nucleating agent to the Shipman process. The nucleating agent was used to reduce the size of the polymer particles, increase their number, and promote rapid crystallization of the polymer. The resulting films were uni-axially or bi-axially oriented before or after diluent extraction. Recently, Clinnton [21] patented the formation of poly(ethylene-*co*-vinyl alcohol) membranes via a process that included film orientation.

Takita et al. [22, 23] at Tonen Corp. formed films from polyethylene in paraffin oil (20 wt-% PE) and bi-axially stretched and annealed films. Takita et al. showed that extraction before stretching (as opposed to after stretching) resulted in films of lower mechanical strength and larger pores. However, they did not offer any explanations for these observations.
None of the patents cited in the preceding two paragraphs report in any detail how the pore size and pore size distribution changed as the result of stretching or how these changes influenced

membrane flux and rejection. The patents do suggest that starting with a given precursor film the final porous structure of the membrane is influenced by the conditions of the stretching (wet *vs* dry; extent of stretching; rate of stretching; stretching temperature; annealing temperature). However, there is, no existing literature describing the modification of membrane pore dimensions via uniaxial stretching, a process that may significantly alter membrane performance characteristics. Recent research [10] has shown that there are advantages to changing the aspect ratio of pores. This project is the first step of an in-depth investigation of membrane stretching as a performance enhancer and includes the development of an appropriate simulation model to enable prediction of performance characteristics from known membrane properties and stretching conditions.

Several mathematical models exist for predicting the change in shape of a void in elastic, plastic, elastic-plastic, and linear viscoelastic materials [24-31]. J.D. Eshelby [24] determined the elastic field surrounding an inclusion in a perfectly elastic solid, noting the special case of an ellipsoid. The predicted stress fields were valid for points close to or far from the void, but not at intermediate distances. McClintock [27] proposed a criterion for fracture in plastic materials with cylindrical voids in an infinite medium, but he ignored interaction effects between voids. Others [32, 33] built on his work by extending it to spherical pores and finite mediums. Gurson [26]proposed a model to predict yield during the stretching of a porous ductile material. The model assumes a rigid, perfectly plastic material and considers the spherically symmetric deformations around a single spherical void and a single cylindrical void. Starting with Gurson's constitutive equation and employing a plastic flow law, Tvegaard [34] proposed a stress analysis model that allows for the merging of neighboring pores as a result of stretching and the breaking of thin regions between pores. Tvegaard applied his model to plastic materials containing periodically distributed cylindrical [34] and spherical pores [35]. Needleman [25] modeled the two-dimensional uniaxial deformation of an elastic-plastic medium containing a double periodic square array of cylindrical voids under plane-strain conditions. Both the effects of geometrical non-linearities resulting from large deformation and physical non-linearities arising from plastic material behavior were included in formulating the problem. Needleman predicted stress distribution, but did not show the configurational change of pores during the stretching process. He also admitted that his model failed well before coalescence of pores.

All of the above studies apply to elastic, plastic, or elastic–plastic materials. Polymers such as those that comprise membranes do not behave according to any of these models; thus, further work is needed. Hashin [36] studied the behavior of linearly viscoelastic heterogeneous material, employing the correspondence principle. Although his study is not specific to voids, it can be extended to that case, as he mentions. Budiansky et al. [29] studied void growth in viscous solids. Mohan and Brust [28] extended this study to determine the effects of elasticity on void evolution in viscous solids, specifically metals that exhibit creep at high temperatures. Polymers exhibit creep behavior, which will be significant in modeling the stretching process, but they exhibit viscoelasticity, which metals do not. Li and Weng [37] studied the void growth of aligned spheroidal voids in linear viscoelastic materials in 1995. Their model of viscoelasticty is arrived at by LaPlace transform of the Eshelby-Moru-Tanank concept of elasticity. Li and Weng extended their study [38] to include composite materials in which inclusions are elastic but the matrix is viscoelastic or viscoplastic, but the case of voids is not discussed. Similarly, Wang and Weng [31] modeled self-similar void growth in linear viscoelastic material at moderate strains. They showed that the condition of self-similar growth depends on the viscoelastic model used. Clements [39] built on the work of Eshelby and Weng by finding an accurate analytical theory for viscoelastic deformation of soft polymers (above the glass transition temperature), which is an improvement on Weng's numerical solution. Clements' work shows that uniaxial deformation of aligned ellipsoidal voids rapidly increases aspect ratio, and more slowly increases void concentration. His work acknowledges the importance of non-linearity at high strains, but does not account for these non-linearities, and does not predict deformation for strains above 80%.

Steenbrink, et al. [40] studied void growth in a finitel element until cell model for a single sphere or cylinder in a visco-plastic material. Most recently, Smit, et al. [41] sought to stabilize the post yield response of polymers by studying the effects of both voids and inclusions. They found that the presence of both voids and inclusions caused the stress to spread out over the material and was successful in stabilizing the post-yield response. These models demonstrate that under uniaxial tension, circular pores change shape to elliptical, however they do not predict coalescence of pores and can only account for pore interactions in a very simple, approximate way.

The materials to be studied here are viscoelastic in their behavior and in order to modify their pore characteristics they will be stretched beyond the linear viscoelasticity region. Linear viscoelasticity is valid for small deformations, usually when the stain is less than 0.5% [42], and assumes that the shape of the material before deformation can be regained once the material has relaxed. The material behavior can be described by a time-temperature shift curve, or master curve, constructed by relaxation experiments and the Williams-Landel-Ferry (WLF) equation. Beyond this linear region, material behavior deviates from this master curve. In addition, it is the goal of this project to create both large and small permanent deformations. Therefore, this project will investigate both a nonlinear viscoelastic constitutive model and/or a viscoplastic model to predict the material behavior.

A constitutive viscoplastic model for PET was proposed by Vigny, et al. [43] to describe plane-strain stretching of PET films for large strains. This model employs a viscoplastic term, which contains several experimentally determined constants. Finite strain models for elastomers have had success predicting the behavior of rubbers at large deformations [44]. This result is relevant because polymers behave like viscous elastomers above the glass transition temperature. Wu and Liechti [45] studied the results from two different models, a pseudo stress model and a pseudo strain model, and were successful in predicting the stress-strain behavior using the pseudo stress models, including the finite viscoelastic model in the finite element program ABAQUS. Although several or all of the models discussed above may be appropriate for modeling the behavior of PC and PET membranes, one of the models this project will employ is the finite strain viscoelastic model, which has already been integrated into the ABAQUS software. The finite strain viscoelastic model in ABAQUS is essentially a pseudo stress model and was shown to be objective[1] [45], which is an essential quality for modeling material behavior. ABAQUS has been used in research to model viscoelastic deformations. Sweeney, et al. [46] employed ABAQUS to solve their constitutive model for the large deformation of polyethylene. ABAQUS has proven to be a successful tool for modeling the behavior of rubbers and polymers.

MATERIALS and METHODS

Track-Etched Membranes

Track-Etched (T-E) membranes made from poly(ethylene teraphthalate) (PET) were kindly donated by Whatman Corporation in the form of 8.5" by 11" sheets. These membranes are produced from Mylar films made by Dupont, and vary in thickness from 13 μm to 23 μm, depending on the pore size. PET membranes with pore sizes of 0.2, 0.4, 0.6, 0.8, 1, 2, 3, and 10 μm were obtained. All PET membranes obtained were hydrophilic.

1 "Objective" is used to identify a constitutive model as being independent on the frame of reference, meaning the answer to the problem does not depend on direction or approach.

Phase Inversion / Phase Separation Membranes

Poly(ether sulfone) (PES) membranes that filter particles with diameter greater than 0.2, 0.8, and 1.2 μm and poly(vinylidene fluoride) (PVDF) membranes that filter particles with a diameter greater than 0.22 and 0.45 μm were kindly donated by Pall Corporation and Millipore Corporation. The PES membranes are hydrophobic and the PVDF membranes are hydrophilic. Membranes that were manufactured on a woven or non-woven backing material were excluded from further study to avoid the complications associated with multi-layer, multi-material structures. Likewise, membranes of a nodular structure (rather than the more common cellular or lacy structure) were eliminated from further study because of the inherent weakness associated with nodular structures.

This report focuses on the results for a Pall Corporation PES membrane of nominal pore size 0.2 μm. When referring to this membrane in this report, the nominal pore size is written with a tilde preceding the number. This is done to reflect the fact that the membranes that were generously provided to us by Pall Corporation are not exactly the commercial 0.2 μm pore size membranes. Instead the membranes used in this research are laboratory samples made by Pall Corp. researchers to approximate the commercial product. Therefore, they may not have exactly the same pore characteristics as the membranes made in the large, full scale production facilities.

Membrane Materials Characterization

T-E Membrane Characterization

Membrane surface characteristics such as pore area, pore major axis, pore minor axis, and porosity were studied using Hitachi S-4500 field emission scanning electron microscope (SEM) and digital image analysis. Two small samples were cut with a razor blade and placed on a stage. The samples were coated with gold palladium, and were then inserted into the vacuum chamber. Five micrographs or pictures were taken of the membrane surface at various locations on each sample for a total of ten pictures. All pictures were taken at the same magnification, which varies from sample to sample in order to get approximately 20 pores per picture.

These pictures, which were saved as digital files, were then analyzed using digital image analysis. Pores that were straight through were shown on the SEM picture as dark spots; however, some pores were slanted. Theses slanted pores were not dark enough for the computer program Scion to recognize as pores, so they were darkened by the operator prior to image analysis. The scale of the picture was inputted to the program so that it could accurately measure pore size and shape characteristics. The image then underwent thresholding, which caused everything but the pore to disappear from the image. The computer could then count the number

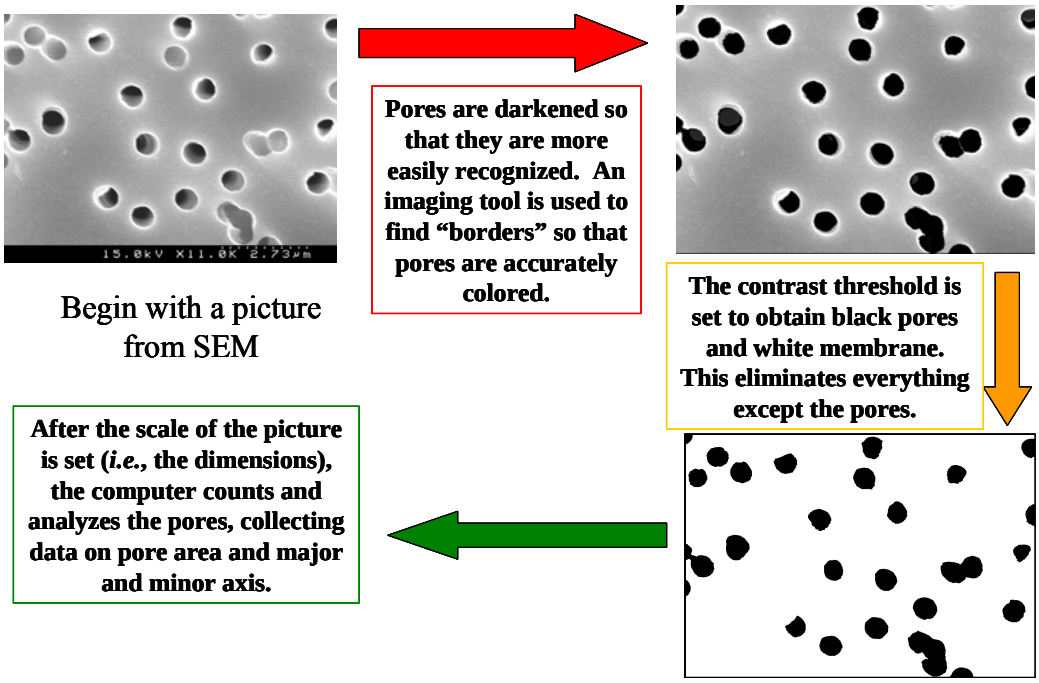

Figure 2: Digital image analysis procedure for TE membranes.

of pores and measure the appropriate characteristics, such as area and major and minor axis. This process is depicted in Figure 2.

PI/PS Membrane Characterization

Scanning electron micrographs was obtained as seven locations for each phase inversion membrane. Twenty five pores on each of those seven images were characterized using Image-Pro Plus, a digital image analysis program by Media Cybernetics (www.mediacy.com). The software was used to measure the major axis length, minor axis length, and angle of orientation relative to the *machine direction* (defined below) for each pore. From the major and minor axis lengths, average membrane aspect ratio and average pore area were calculated. Pore area was calculated by assuming the pore is elliptical in nature, which under most circumstances was proven to be a reasonable assumption.

Error Calculation in Surface Pore Characteristics

A statistics program, JMP (http://www.jmp.com/), was utilized to determine the error in calculating pore area, major and minor axis, and aspect ratio. As described above, many pictures were taken of each sample and analyzed using the digital image analysis procedures described above, which results in the reporting of each pores area and major and minor axis. These numbers, along with aspect ratio calculated from the major and minor axis, were entered into the JMP program in groups according to the picture from which each set of data came. JMP compares the data by picture and eliminates any that seem to be significantly different from the rest of the group according to a student's t-test. Once these outliers have been eliminated, JMP calculated the mean values of area, major and minor axis, and aspect ratio, and reported a 95% confidence interval. This interval is used in this report as the error associated with the calculation of these numbers.

Stretching Experiments

Equipment

A biaxial stretcher (www.inventurelabs.com) was donated by 3M Company. A picture of this equipment is shown in Figure 3. Upon instillation of the device, some of its controls and components were not fully operational or not up to the desired standard of accuracy. Therefore, a new electric stepper motor was installed to replace the existing hydraulic motor. A new load module was also installed, along with a potentiometer to measure strain and strain rate, and new heating plates were installed. All systems were automated using Lab View software. The pneumatic gripping system is original to the machine, as is the pantograph mechanism.

Figure 3: Biaxial stretcher.

Sample Preparation

A membrane sample to be stretched was cut using a razor blade. The sample length was cut to be approximately 10 cm in width and approximately 11 cm or more in length. Each end of the sample was wrapped around a metal bar to help assure proper alignment and to evenly distribute gripping force over the width of the membrane.

Experimental Procedure

The sample was placed in the machine with the two bars secured in the gripping mechanisms. The two sides not wrapped around the bars were left unconstrained. Nitrogen gas was used to apply pressure and grip the two ends of the membrane sample. The sample was them pre-tensioned, meaning that the gripping mechanism attached to one end of the sample was moved out just enough to make the sample taut. Movement of the grip is via a motor drive. The top of the box then was closed and the heating plate turned on. After the plates reach the desired temperature, the sample was left in the box for 30 minutes to ensure that the sample has also reached the desired temperature. The appropriate strain rate was chosen, and the distance required to reach the desired strain was calculated. This strain was then applied to the sample. Once the sample had reached the desired strain, it was annealed at either the same or higher temperature for 10 to 15 minutes. The box was then opened and the sample allowed to cool. The sample was them removed and measured with a ruler accurate to 0.05” in order to determine the actual strain obtained. All samples were stretched in the machine direction, meaning that all samples were stretched in the direction that the membrane was made.

Model Simulations

ABAQUS and Choice of Constitutive Model

The finite element simulation program ABAQUS (www.hks.com) was chosen to perform simulations of the stretching process. An appropriate constitutive model must be chosen to describe the material behavior during stretching. This model has to be able to take into account the viscoelastic nature of the polymers being used, non-linear geometric effects due to large

strain, and permanent deformations. One of the constitutive models chosen to begin simulations is a finite strain hyperelastic viscoelastic model that has already been integrated into ABAQUS. Another is a viscoplastic model. Both of these models require the coefficients of the Prony series, which describes the viscoelastic part of the model, and each will require some additional parameters.

Prony Series Construction

The Prony series can be extracted from the master curve that describes a material's behavior. This master curve can be constructed from a series of relaxation experiments performed at various temperatures. A pre-determined strain is applied to the sample, and the sample is held there while force is measured. This force is translated to stress by dividing by sample thickness and width, as shown in Equation 1.

$$\sigma(t) = \frac{F(t)}{\text{width} \cdot \text{thickness}} \qquad (1)$$

This stress is translated to relaxation function by dividing by the constant strain applied to the sample, as shown in equation 2.

$$E(t) = \frac{\sigma(t)}{\gamma} \qquad (2)$$

Using the WLF equation, the individual experiments are shifted to form a master curve, qualitatively shown in Figure 4. The shift factor, a_T, is calculated by equation 3, where is reference temperature is taken to be 50°C above the glass transition of the polymer being studied and T is the temperature at which the relaxation experiment took place.

$$\log(a_T) = \frac{86.6 \cdot (T - T_{reference})}{101.6 + (T - T_{reference})} \qquad (3)$$

Reduced time, t', is given by equation 4.

$$t' = \frac{t}{a_T} \qquad (4)$$

The log of the relaxation function is potted against the log of reduced time for experiments at various temperatures, and the curve in Figure 4 is obtained. This curve can be described mathematically as the sum of a series of exponential terms, called the Prony series shown in equation 5. The coefficients of these terms are required by ABAQUS to describe the material behavior.

$$\mu(t) = \mu_e + \sum_{k=1}^{n} \mu_k \cdot e^{\frac{-t}{\tau_K}} \qquad (5)$$

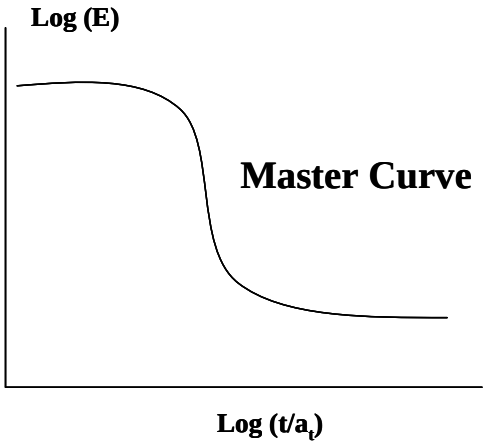

Figure 4: Qualitative master curve.

Model Simulation

To begin, a film with one pore located at the center is stretched and its final pore size characteristics are predicted. As shown in Figure 5, the stress of greatest magnitude occurs on the outside wall of the pore. This pore can be compared directly to an experimentally stretched pore that is not interacting with other pores, but before this can occur, it the extent of poer interaction must be determined. The next step is to simulate the stretching of a film with two pores in it. The distance between pores, as well as their orientation relative to the stretch direction, will be varied to determine the extent of their interaction. Once this is complete, pores can be added to the simulation until a representative section of the membrane can be stretched in simulation and compared to the results of SEM and digital image analysis of experimentally stretched samples. A picture of this procedure can be seen in Figure 5.

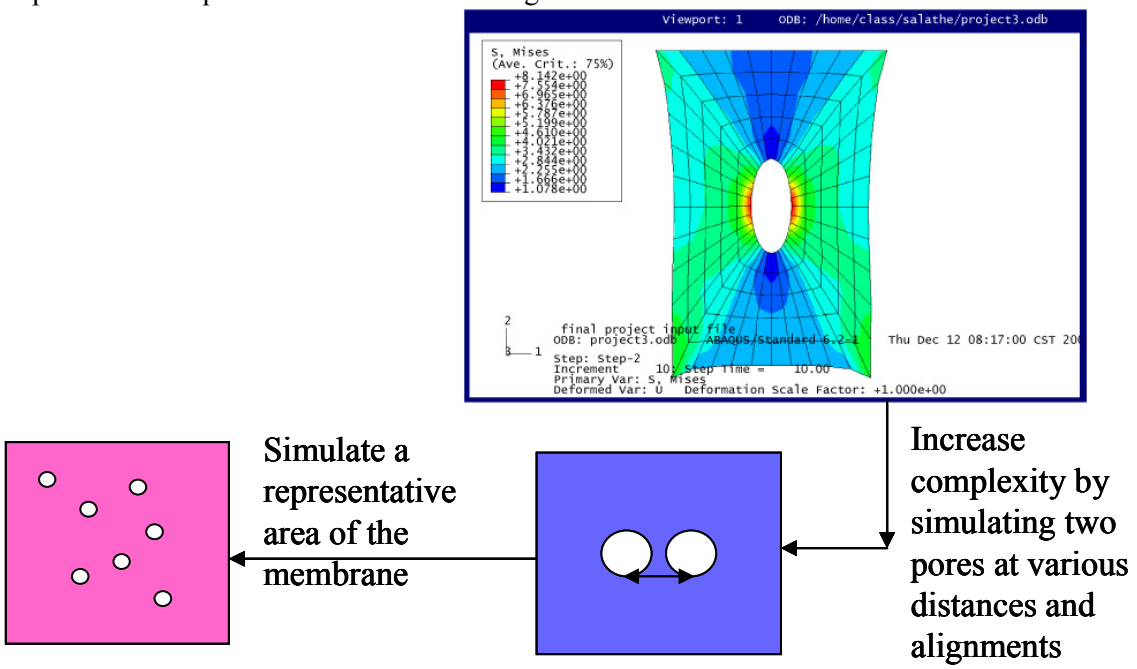

Figure 5: Graphical output from ABAQUS simulation, and simulation procedure.

Sample Preparation for Permeation Studies

Membrane Sample Preparation and Equipment

Figure 6: Permeation module

Two dead-end permeation modules were used for permeation experiments. Both are Micron models supplied by Millipore. One is a 15 mL module with a 25 mm sample diameter, and the other is a 75 mL module with a 45 mm sample diameter. The larger module can be used as a stirred module, while the smaller module cannot. The modules are hooked up to a reservoir, which holds up to 5 L. The reservoir opens at the top so that suspensions can be added. The top is sealed, and the reservoir is pressurized with nitrogen gas. The pressure is controlled by a digital controller (Praxair, Model GC12) with a digital

pressure gauge in line. Figure 5 shows a picture of the permeation module. PET membrane samples were cut using a die of the appropriate size and a razor. The pattern was marked on the membrane with a marker, and them the sample was cut just inside the marking with a razor blade. The PI/PS membranes were marked with the same die, but cut using scissors. Then the sample was placed in the permeation module. The PET membranes did not need to be wetted before being placed inside the permeation module. PES membranes needed to be wetted with isopropanol before being placed in the module.

Particulate Challenge Sample Preparation

Particulate challenge experiments were performed with two types of particles. Min-u-sil was the first particle used in membrane rejection experiments. Min-u-sil 5 is an irregularly shaped particle that is 99.2% silicon dioxide. Min-u-sil 5 has a broad particle size distribution with 88% of the particles having a diameter between 0.8 and 2.5 μm with a median size of 1.7 μm, shown in Figure 7. A picture of these particles is shown in Figure 8. The particles were used to test membranes with pore sizes of 1, 2, and 3 μm. Similarly, Min-u-sil 30 was used to test the 10 μm pore size. Min-u-sil 30 is similar in particle size distribution to the Min-u-sil 5 described above, but with larger particles. Cross-linked polystyrene beads (Duke Scientific Corporation; give contact information) of size 2.02 μm were used to test the 2 μm pore size membranes, while beads of 0.17, 0.3, 0.52, and 0.65 μm were used for various membranes of appropriate sizes. All beads come as aqueous suspensions in 15 mL bottles that are 10% solids by weight. A volumetric flask is filled with the desired amount of pure (Milli-Q) water. The bottle of suspended beads is sonicated, and the appropriate volume of particle suspension is removed from the bottle and transferred to the volumetric flask using a Rainin electronic digital pipette. This new suspension was inverted several times to ensure good mixing of the suspension.

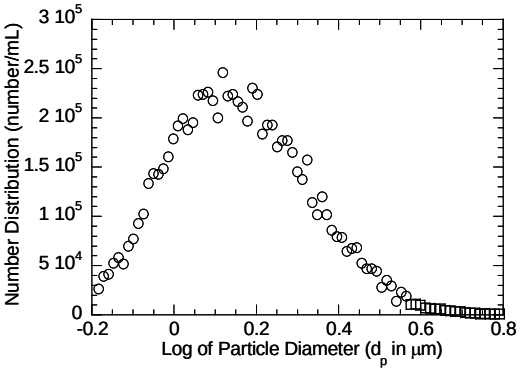

Figure 7: Min-u-sil particle size distribution.

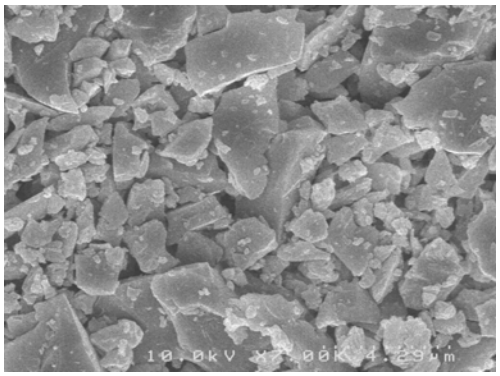

Figure 8: Min-u-sil 5

Protein Fouling Sample Preparation

A 1 g/L bovine serum albumin (BSA, obtained from Sigma-Aldrich, St. Louis, MO, catalog #A-7906, batch #123K0646) solution was used as the model permeate in the protein fouling experiments. The batches were prepared by slowly adding 1 g BSA to 3 L of phosphate-buffered (pH= 7.4) water (powder phosphate buffer was obtained from Sigma-Aldrich, St. Louis, MO, catalog #P-3813; water was obtained from an 18.2 MΩ Millipore Milli-Q plus system) while stirring at an approximate speed of 200 rpm. Once all of the BSA was added, the solution was stirred for an additional 30 minutes.

Permeation Experimental Procedure

Pure Water and Particulate Challenge Experiments

A suspension of the appropriate particle concentration was mixed to a total volume of 1 to 1.5 L. After the membrane was placed in the module and sealed with the o-ring, 1 L of pure water, from a Milli-Q system, was added to the reservoir and the reservoir was sealed. An appropriate pressure, between 6 and 20 psi, was chosen, and the pure water was forced through the membrane and the permeate was collected in a series of volumetric flasks. Time was recorded at regular volume intervals to determine the flux through the membrane. While the membrane was still wet, the particulate suspension was added to the reservoir and the reservoir was closed. The pressure was increased again and the suspension was forced through the membrane. Permeate samples were collected at regular intervals, and time was recorded at each interval.

Protein Fouling Experiments

The BSA solution was carefully poured into a sealed reservoir. A 1 gallon, 316 stainless steel, wide-mouth vessel ordered from Advantec MFS (Dublin, CA; Pt. #470140) was used in all protein and oil-water emulsion testing. A transmembrane pressure difference of 10 psi was used in dead-end filtration for all protein fouling experiments. The filtration module was stirred at approximately 300 rpm. A balance linked to a personal computer allowed for the measurement of total permeate mass every 10 seconds.

Suspension and Solution Characterization

Turbidimeter

One method used to characterize the particle content in the feed and permeate is to measure the turbidity. A model Hach Ratio/XR Turbidimeter was used in this study. This instrument shines a light through the solution or suspension and then measures the amount of light deflected at a 90^{o} angle to determine the turbidity or cloudiness of the suspension and reports this measurement in nephelometer turbidity units (NTU). Samples are measured by pouring the suspension into a clear glass tube, making sure the outside of the glass tube is clean, and inserting the tube into the turbidimeter and closing the top. Readings are taken from samples that were saved at regular intervals over the course of the permeation experiment. These samples are mixed gently to assure uniformity of particle concentration while avoiding the formation of bubbles.

Coulter Counter

Another way to characterize permeate concentration is to measure the particle size distribution. In this research, a model Beckman-Coulter Multisizer 3 (www.beckmancoulter.com) is used. This instrument counts and measures the number and size of particles in the permeate, so that particle size distribution in the permeate can be known.

A Coulter Counter draws a sample in a salt solution through an aperture across which a constant current exists. As the sample flows through the aperture, each particle causes an increase in the electrical resistance which leads, with the constant current, to a voltage increase that is proportional to the particle volume. A pulse height analyzer then counts and sorts the voltage pulses into size bins. A 30 μm aperture tube is calibrated to accurately measure particles with a diameter or equivalent spherical diameter between 0.6 μm and 12 μm. The 100 μm aperture tube can measure particles in the range of 2 μm to 40 μm. The pulse height distribution information is translated via the calibration curve into a particle size distribution. Data from the

Coulter Counter was used to determine the effect of membrane stretching on particle rejection over a range of particle sizes.

UV Spectrophotometer

A sample of both the feed and the final permeate solution was analyzed using UV spectroscopy to define rejection characteristics of the membrane for organic proteins. Approximately 2 mL of the feed and permeate solutions, respectively, was collected and placed into a glass cuvette, which was in turn inserted into a Shimadzu UV-Visible Bio-Spec Mini Spectrophotometer. It has been well documented in the literature that our model protein, BSA, absorbs UV light at a wavelength of 280 nm. Using the Shimadzu UV spectrophotometer set to determine absorbance at 280 nm, we have made an absorbance calibration curve using set protein solution concentrations. When running an actual test, the UV spectrophotometer will use this curve to determine the exact protein concentration, which it reports to the nearest ten-thousandth of a gram per liter. Testing only requires a few seconds to complete per sample.

RESULTS and DISCUSSION

Pre-Stretched Membrane Materials Characteristics

Track-Etched Membranes

Pore characteristics were analyzed for all PET membranes before stretching. Pore area, pore major axis, and pore minor axis were measured per the procedure described in the previous section. Although the method of manufacturing T-E membranes produces circular pore entrances, the aspect ratio of the non-stretched samples is greater than one due to the overlapping of pores, as shown in Figure 9. Table 1 gives a summary of these results for all the PET membranes used in this project, including 95% confidence limits, which are reported for all membrane surface measurements taken. Reported area is defined as the average area of an individual pore. These results were used to compare stretched samples with their non-stretched state and determine the change in pore characteristics.

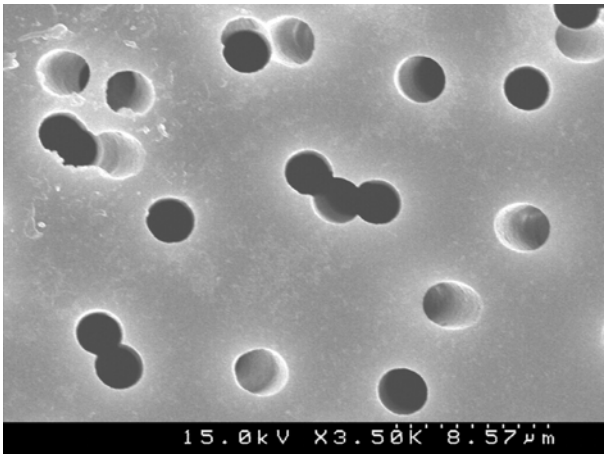

Figure 9: Typical track-etched membrane showing overlapping pores.

Table 1: Surface pore characteristics for non-stretched track-etched membranes.

Pore Size (μm)	Area (μm^2)	Major Axis (μm)	Minor Axis (μm)	Aspect Ratio
0.6	0.26 ± 0.02	0.66 ± 0.03	0.53 ± 0.01	1.23 ± 0.05
0.8	0.44 ± 0.03	0.81 ± 0.04	0.67 ± 0.02	1.24 ± 0.07
1	0.71 ± 0.03	1.02 ± 0.04	0.89 ± 0.01	1.18 ± 0.06
2	2.22 ± 0.12	1.87 ± 0.08	1.48 ± 0.04	1.26 ± 0.04
3	6.02 ± 0.67	3.16 ± 0.29	2.39 ± 0.04	1.31 ± 0.11
10	65.41 ± 3.98	10.11 ± 0.58	8.20 ± 0.12	1.24 ± 0.07

PI/PS Membranes

The non-stretched ~0.2 μm PES membrane was characterized using the procedure described in the Methods and Materials section. The results for the pore characteristics and membrane thickness are reported in Table 2. Comparison of the results reported in Table 2 to those reported in Table 1 shows that the PI/PS membrane has a significantly larger pore area than all but the largest pore size PET membranes. The ~0.2 μm PES membrane also has a larger initial aspect ratio than the track-etched membrane. Both of these differences are a consequence of the different methods of manufacturing the membranes, and both of these differences have significant impact on the changes the membrane will undergo when stretched.

Table 2: Surface pore characteristics of non-stretched ~0.2 μm PES.

Aspect Ratio	1.68 ± 0.08
Area (μm^2)	5.6 ± 0.3
Major Axis Length (μm)	1.7 ± 0.4
Minor Axis Length (μm)	1.0 ± 0.2
Membrane Thickness (μm)	145 ± 2
Hydrophobocity	Hydrophobic
Major Axis Angle	Random

In addition, the membrane was characterized using differential scanning calorimetry (DSC). The DSC results are reported below in Table 3. All of these characterizations were performed to provide base line statistics so the effects of stretching on membrane properties could be monitored.

Table 3: DSC results for ~0.2 μm PES.

	Melt Temperature (°C)	ΔH Fusion (mW)
Non stretched	180.5	23.3
100% Stretch	182.3	24.5

Post-Stretched Membrane Materials Characteristics

Track-Etched Membranes

PET membranes with pore sizes ranging from 0.2 to 10 μm were stretched at various combinations of temperature, strain rate, and overall strain. Temperatures ranging from 80 to 180°C were used, and strain rates of 0.025 and 0.25 cm/s were attempted. As discussed below, some membranes were only successfully stretched to small strains, such as 5 or 10%, and others were stretched up to 32% before breaking. SEM micrographs were taken of all samples, and these micrographs were analyzed using the digital image analysis technique discussed in the previous section.

The PET membranes with pore size 0.4 μm were stretched to a maximum strain of 5% at 160°C and a strain rate of 0.025 cm/s. The results of this stretch were that area decreased by 6% and aspect ratio increased by 5%. PET membranes with 0.8 μm pore sizes were stretched 15% at 160°C and 0.025 cm/s before breaking, corresponding to a 43% increase in area and aspect ratio.

PET membranes with pore sizes of 0.6 μm were stretched to a maximum strain of 29% at 160°C and 0.25 cm/s, which corresponds to a 102% increase in aspect ratio and a 39% increase in area. Figure 10 shows a picture of (a) an non-stretched membrane, and (b) a 29% stretched sample. Intermediate stretches of 14 and 26% were also obtained and analyzed. Table 4 shows the resulting change (relative to the non-stretched membrane) in pore area, major axis, minor axis, and aspect ratio for these membranes. Shown in Figure 11 are the aspect ratio–strain and area–strain relationships for the 0.6 μm PET membranes. Aspect ratio seems to be proportional to strain up to the point of breaking, whereas area does not follow such a simple relationship. This trend is generally evident in all the other PET samples tested and reported below. The nature of these two relationships needs to be explored further in future work in order to assist manufactures of T-E membranes in their attempts to modify membranes via stretching.

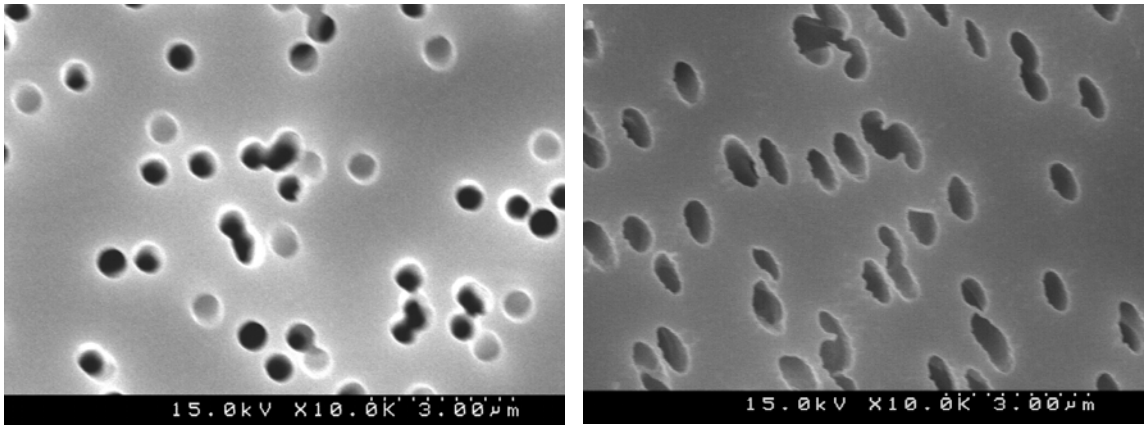

Figure 10: Non-stretched and 29% stretched 0.6 μm PET membrane.

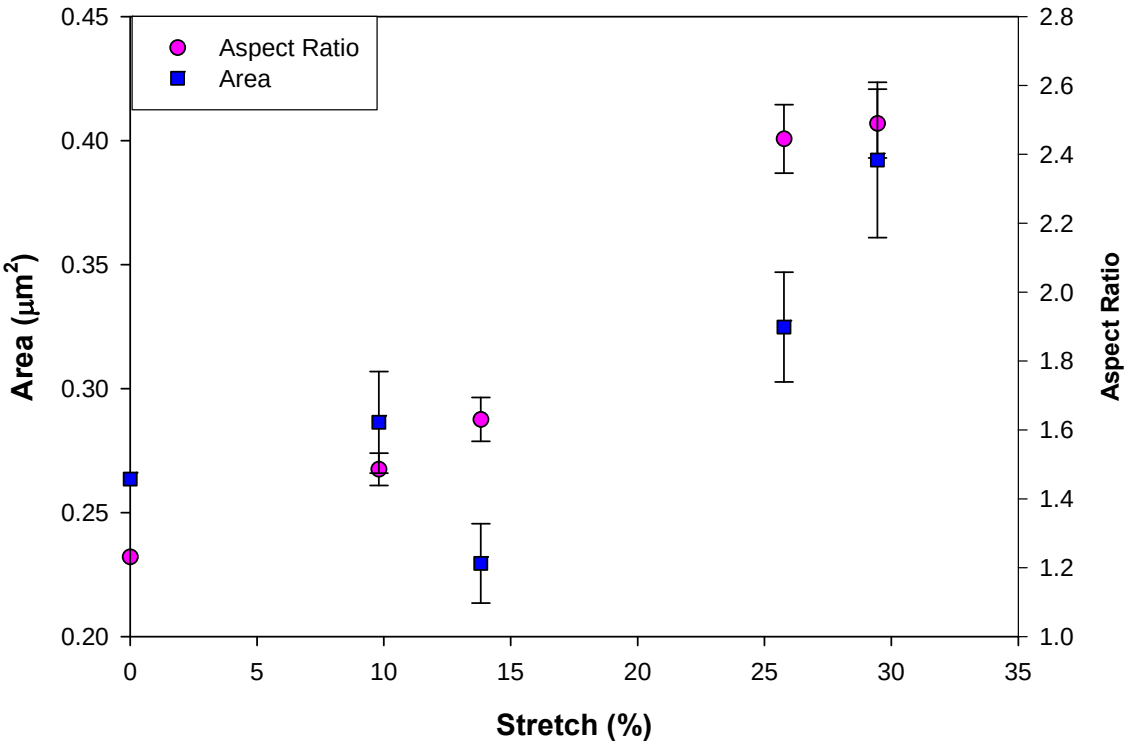

Figure 11: Area and aspect ratio shown as a function of strain for 0.6 μm PET membranes.

Table 4: Surface pore characteristics for PET membranes at various strains.

Strain	% change area	% change major	% change minor	% change aspect
0.6 μm PET Membrane				
14%	13% ± 7%	12% ± 4%	-17% ± 3%	32% ± 4%
26%	23% ± 7%	58% ± 4%	-23% ± 4%	99% ± 4%
29%	49% ± 8%	66% ± 4%	-15% ± 4%	102% ± 4%
1 μm PET Membrane				
11%	31% ± 5%	55% ± 4%	-14% ± 1%	78% ± 2%
13%	8% ± 4%	32% ± 2%	-15% ± 1%	54% ± 3%
21%	56% ± 4%	49% ± 1%	-4% ± 2%	44% ± 3%
22%	29% ± 4%	53% ± 2%	-14% ± 1%	72% ± 3%
2 μm PET Membrane				
12%	43% ± 8%	37% ± 3%	1% ± 3%	32% ± 3%
22%	32% ± 6%	45% ± 3%	-9% ± 4%	65% ± 4%
24%	34% ± 6%	49% ± 3%	-11% ± 3%	71% ± 3%
27%	65% ± 4%	98% ± 3%	-16% ± 2%	151% ± 3%
32%	77% ± 10%	89% ± 4%	-3% ± 3%	100% ± 4%
3 μm PET Membrane				
11%	-3% ± 9%	3% ± 5%	-8% ± 4%	16% ± 4%
13%	13% ± 8%	18% ± 5%	-7% ± 3%	29% ± 4%
18%	5% ± 8%	23% ± 5%	-13% ± 4%	47% ± 5%
21%	23% ± 9%	32% ± 4%	-5% ± 4%	44% ± 4%

PET membranes with pore size 1 μm were stretched up to a maximum of 22% at 140^{o}C at a strain rate of 0.25 cm/s before breaking. Table 4 shows the resulting pore characteristics of some of the stretches obtained for this sample. Figure 12 shows a picture of (a) a non-stretched and (b) 22% stretched membrane. The relationships between aspect ratio and strain and area and strain are shown in Figure 13.

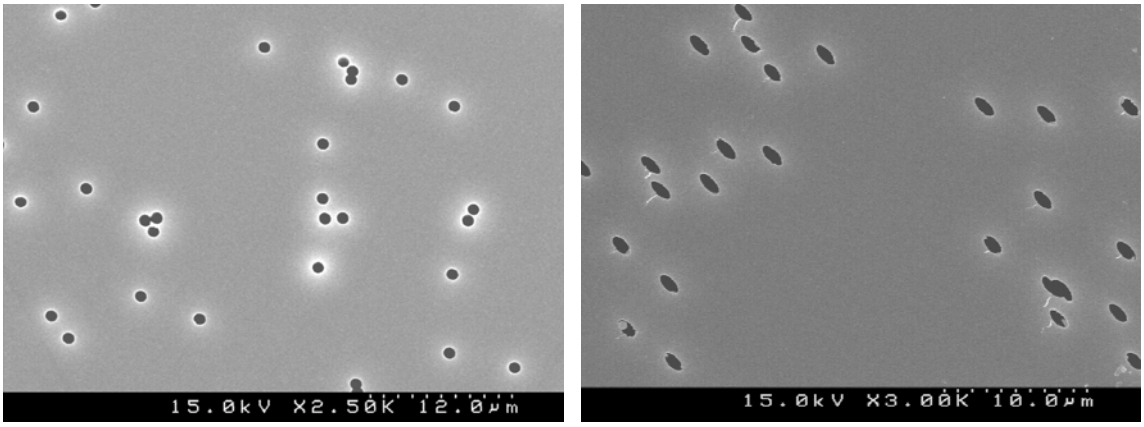

Figure 12: Non-stretched and 22% stretched 1 μm PET membrane.

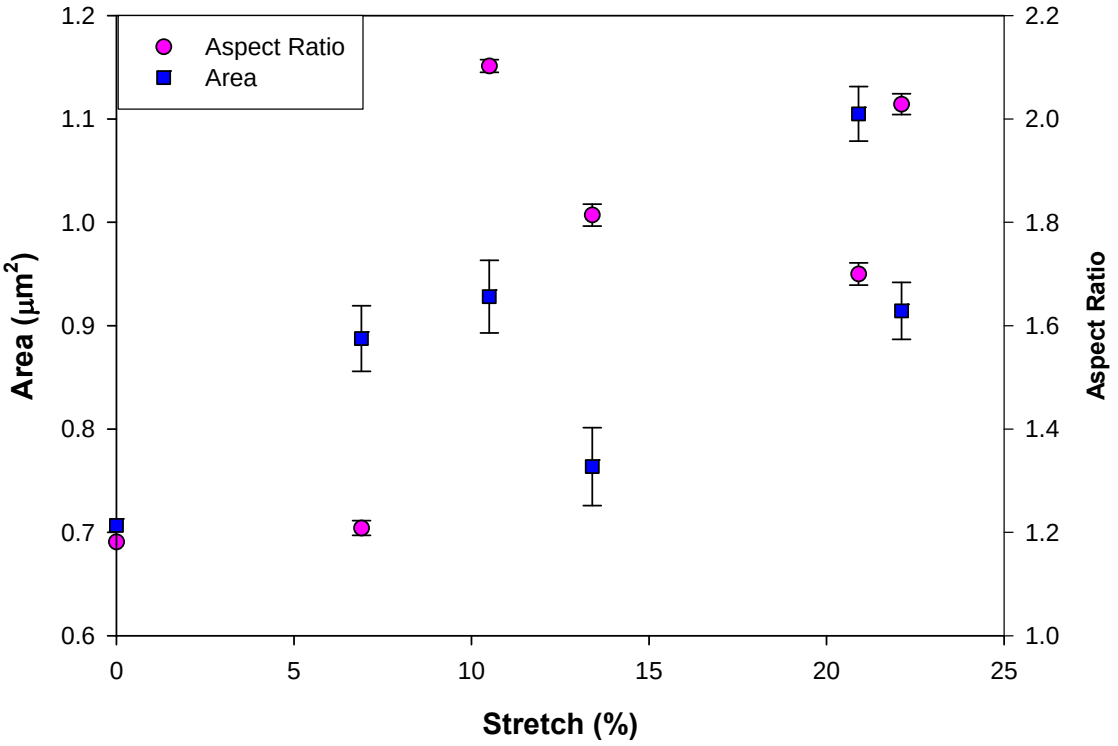

Figure 13: Area and aspect ratio shown as a function of strain for 1 μm PET membranes.

The PET membranes with pore size of 2 μm were stretched up to 32% at 160°C and 0.25 cm/s, the highest overall strain obtained for any T-E sample. Table 4 gives the results of this and other intermediate stretches for this sample. Figure 14 shows a picture of both (a) an non-stretched and (b) a 32% stretched sample. Shown again in Figure 15 is the trend between aspect ratio and stretch and area and stretch.

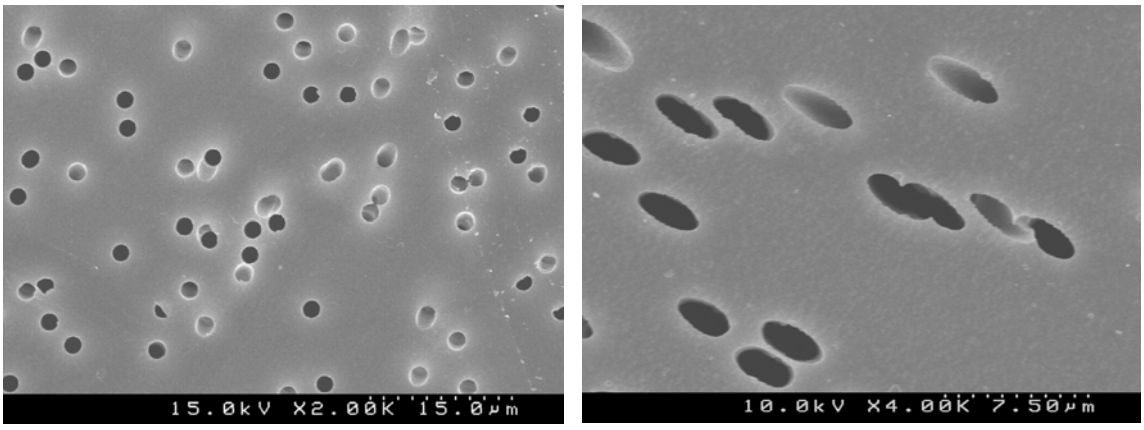

Figure 14: Non-stretched and 32% stretched 2 μm PET membrane.

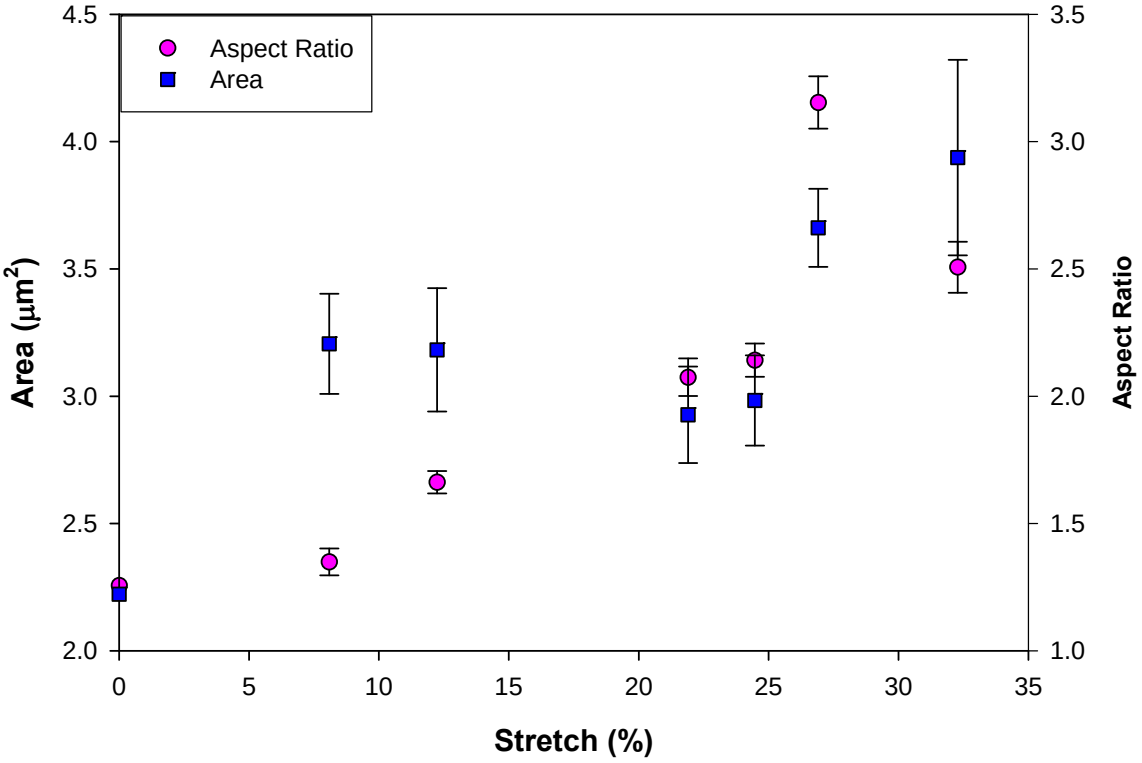

Figure 15: Effect of strain on area and aspect ratio for 2 μm PET membranes.

3 μm PET samples were stretched up to 21% at 160°C and 0.25 cm/s before breaking. Table 3 gives a summary of the results of this stretch and other intermediate stretches for this sample. Figure 16 gives the relationship between strain and both aspect ratio and area.

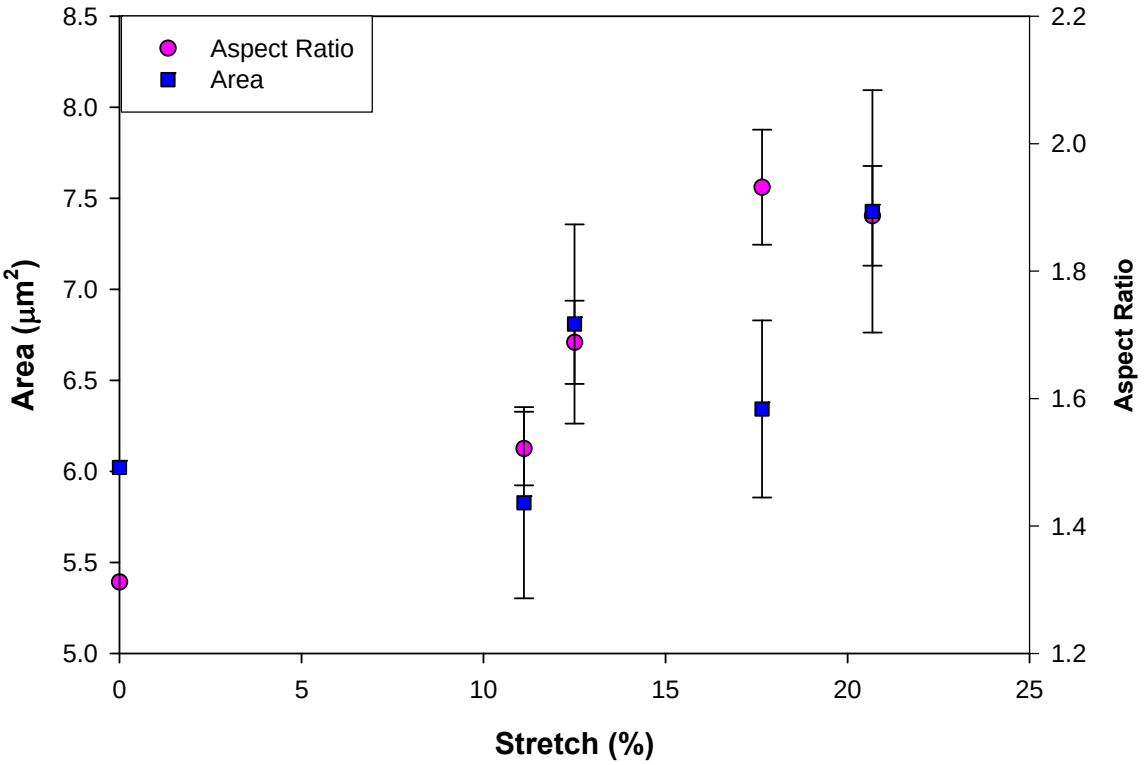

Figure 16: Effect of strain on area and aspect ratio for 3 μm PET membranes.

10 μm PET samples were stretched up to 18% at 100°C and 0.025 cm/s, which resulted in a 69% increase in area and a 53% increase in aspect ratio.

The results presented in Table 4 and Figures 11, 13, 15, and 16 indicate that in general stretching PET membranes decreases the minor axis, increases the major axis, increases the aspect ratio, and in most cases increases the area. The scatter in the data clearly indicates that more experimentation is needed to improve the quality of the data and to quantify the aspect ratio–stain and area–strain relationships. Because of the desire of the RAB to push ahead and test membranes, time was not taken during this project to improve these materials science relationships; however, future plans under separate sponsorship should resolve these issues.

Figure 17 demonstrates that when all of the available date for all of the T-E membranes is combined, the aspect ratio is proportional to overall strain, albeit with some scatter. Such a simple relationship is not evident for pore area and the other pore characteristics. Again, future work should more clearly establish such relationships if they do exist.

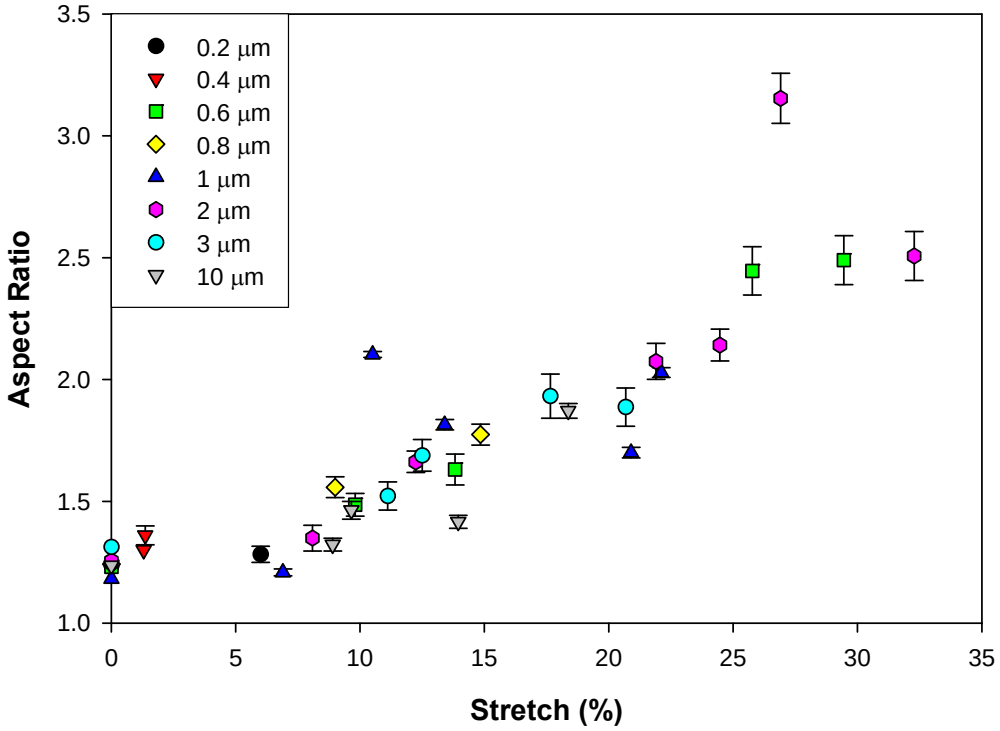

Figure 17: Effect of strain on aspect ratio for all PET membranes.

Although it is know that strain rate and temperature will affect the shape and size of pores after stretching and the maximum strain possible, these effects have not been quantified within the time frame and redefined scope of this project. An experimental design is being formed to quantify these effects in the future.

PI/PS Membranes

The primary membrane analyzed in this aspect of the study has been a poly(ether sulfone) (PES) membrane that is characterized by the manufacturer as having 90% rejection of particles of diameter greater than or equal to 0.2 μm. This membrane was stretched at strains ranging from 14% to 150% at temperatures of 80°C to 160°C and strain rates from 0.1 to 6 cm/s. Pore characteristics were analyzed using SEM, membrane polymer properties were studied with DSC, and membrane porosity was measured using the method outlined above.

DSC was used to detect the melt temperature and latent heat of fusion for the material (indicative of the degree of crystallinity.) The results reported in Table 3 indicate that stretching the PES membrane did not change the melt temperature or the degree of crystallinity.

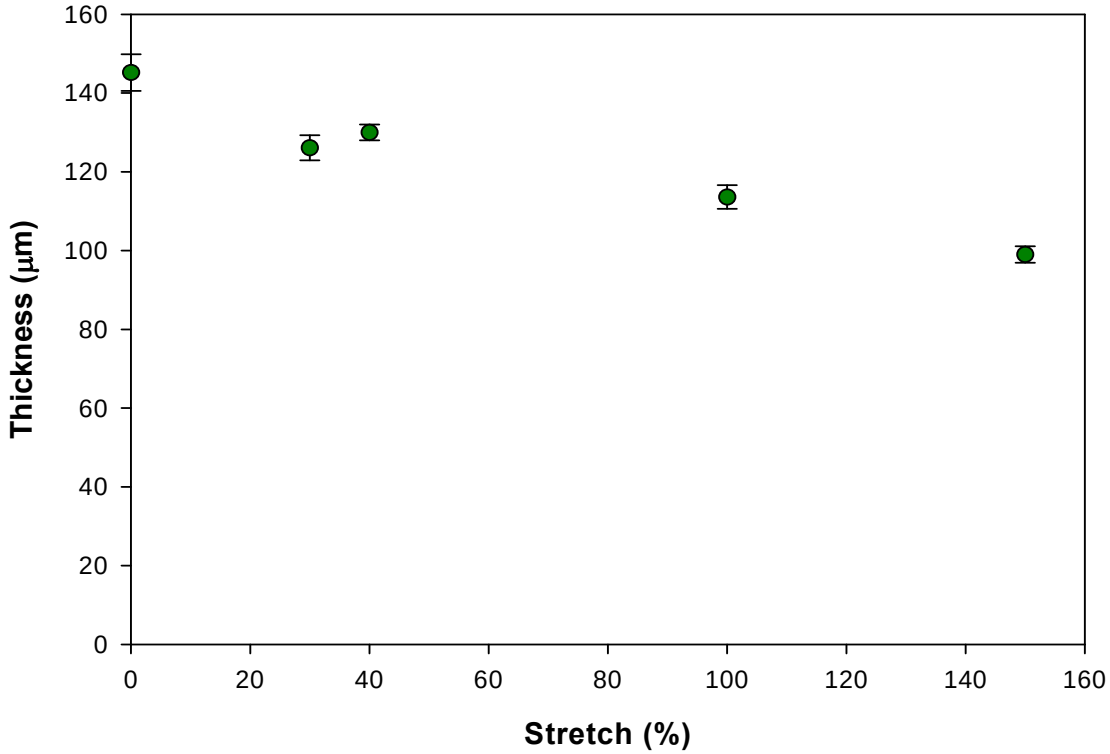

Figure 18: Effect of strain on membrane thickness for ~0.2 μm PES membrane.

Figure 18 shows that membrane thickness decreases linearly with increased strain. This will result in a greater membrane flux due to the fact that flux is inversely proportional to the membrane thickness, but may result in the weakening of the membrane. Future work must be completed to determine if a stretched membrane loses mechanical strength when stretched. This loss could result in an inability to withstand the forces of back-pulsing and cross flow filtration.

The ability of polymer chains to rearrange when subjected to strain depends on the process temperature, the strain rate, and the degree of crystallinity of the polymer. In general, higher temperatures and lower strain rates should allow the polymer molecules time to rearrange during the stretching process. In terms of modification of membrane pore structure via stretching, through the appropriate choice of strain rate and process temperature, it should be possible to increase the total strain possible before breakage; this is particularly important as a means of avoiding the breakage of polymer segments between pores and the merging of pores. While the redefined objectives of this project did not allow full exploration of the effects of stretch temperature and stain rate, some preliminary work was completed. Figure 19 shows that at a specific temperature of 160°C the membrane average pore aspect ratio showed a dependence on the rate at which stretching occurred. All membranes were stretched to equal strains of 100%. A sharp decline in aspect ratio is seen above a strain of 1.5 cm/s at 160°C. Furthermore, a ~0.2 μm PES membrane being stretched at 0.1 cm/s and 160°C can be stretched to a strain of approximately 180% before fracturing**;** however**,** the same membrane stretched at the same rate

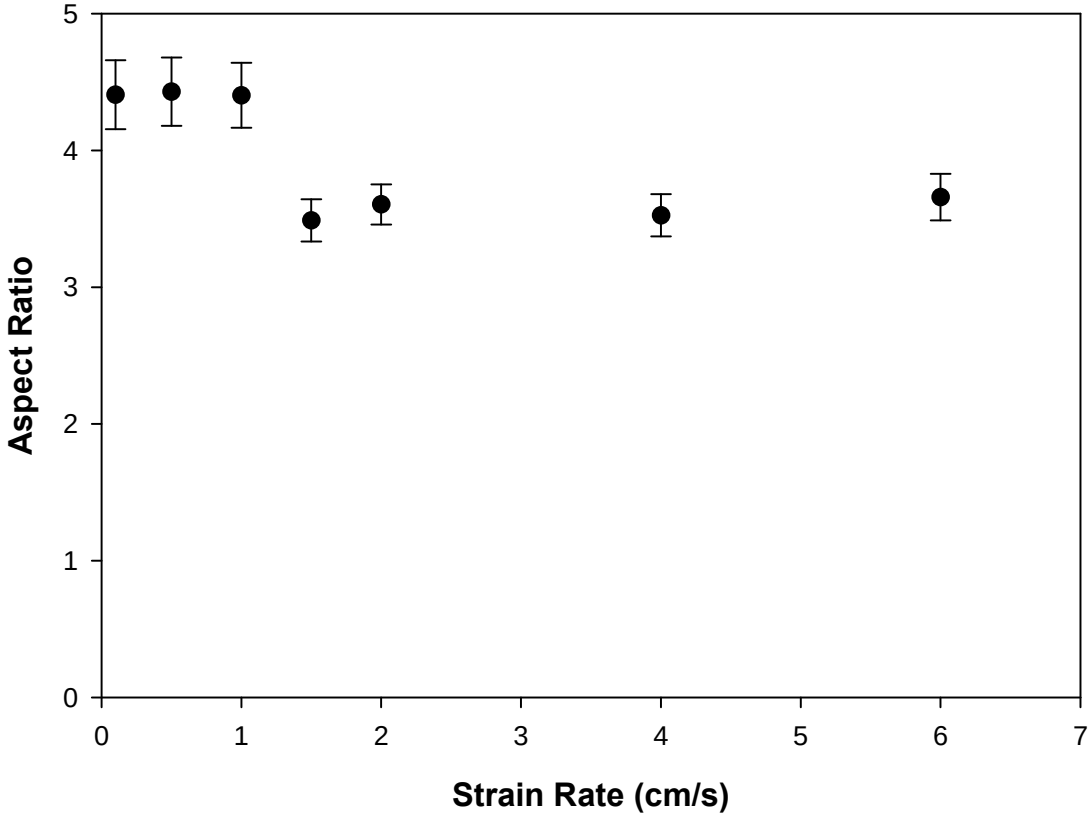

Figure 19: Effect of strain rate on pore aspect ratio for ~0.2 μm PES. Membrane was stretched at 160°C in all cases to a total strain if 100%.

but at 80°C broke at approximately 120% strain. These preliminary results clearly indicate the need for a thorough study of the effects of stretching temperature, strain rate, and polymer relaxation rates. Meanwhile, to advance the present study in a timely fashion, the project moved ahead with a set of conditions that were able to produce membranes that could be used for

permeation studies. Specifically, all membranes reported below ~0.2 μm PES membranes stretched at a temperature of 160°C and a strain rate of 0.1 cm/s. These conditions had resulted in repeatable data in the preliminary experiments and had affected significantly the final pore aspect ratio.

~0.2 μm PES membranes stretched at 160°C and 0.1 cm/s shows a non-linear increase in the aspect ratio up to the point at which the membrane fractures, as shown in Figure 20. One possible explanation for the non-linearity and leveling off of Figure 20 is the transition from elongation of pores at low strains to a combination of pore elongation and the breaking of strands between pores (and thus the merging of pores) at higher strains. A thorough study of the breaking of walls or strands between pores needs to be undertaken in the future to understand fully the relationship between aspect ratio and strain.

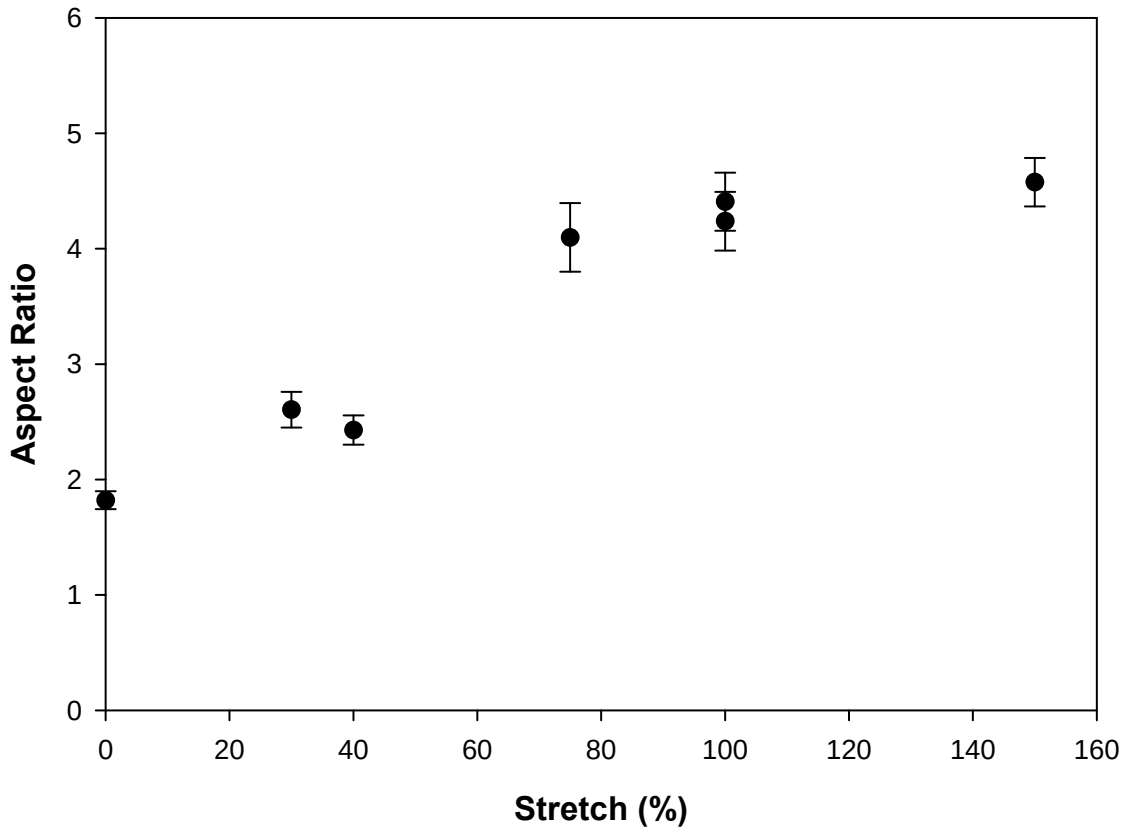

Figure 20: Effect of stretching on aspect ratio for ~0.2 μm PES membrane. All stretching performed at 160°C and 0.1 cm/s.

The initial membrane pore structure prior to stretching the pores are slightly elliptical with a random orientation. Figure 21 shows the major axis angle for 175 pores within a membrane at various levels of strain. This angle is arrived at by using the digital image analysis software discussed previously. A line is drawn through the major axis of the pore and the angle of that line relative to the stretch direction is reported by the software. The 0° line on the ordinate of the graph represents the direction of strain. Therefore, a pore with a major axis pore angle of 90° would have its direction exactly perpendicular to the direction of strain. The aligning of the pores in the direction of strain begins to be evident with as little as a 40% strain. When strains

reach 100% and 150%, as shown in Figure 22, pore alignment is almost completely uniform in the direction of strain. Future studies will investigate the impact of pore alignment on membrane performance in cross-flow microfiltration.

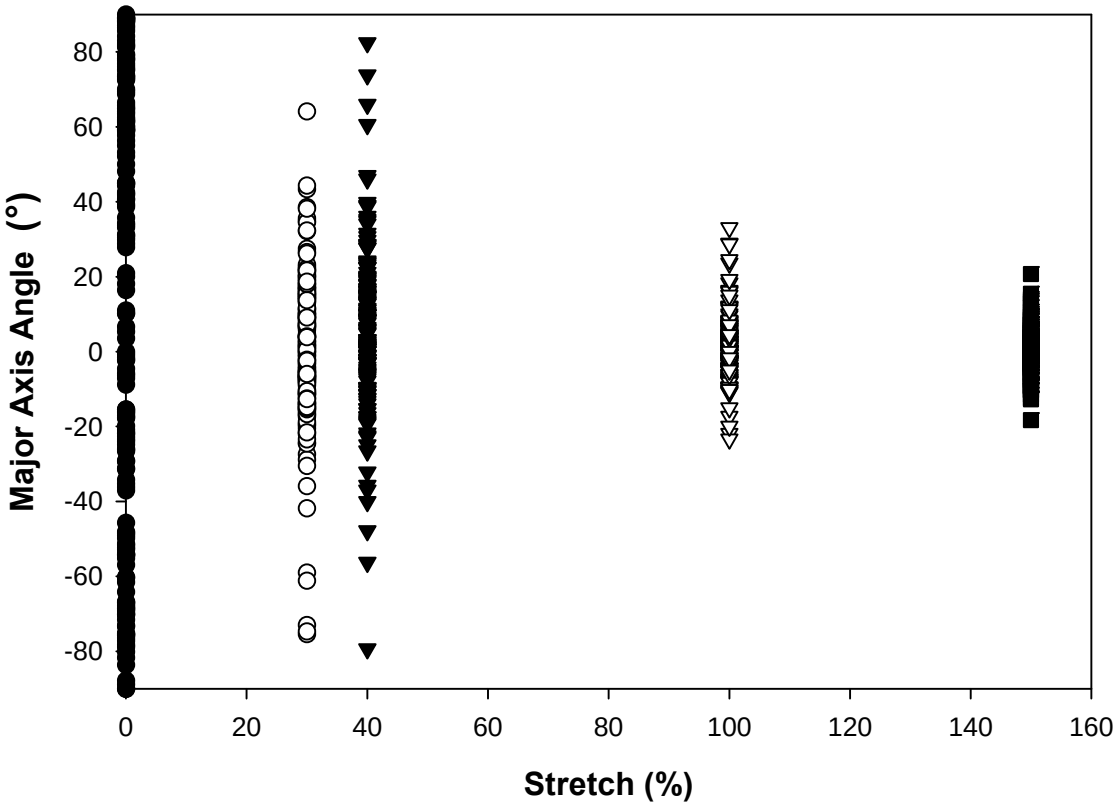

Figure 21: Effect of stretching on pore alignment for ~0.2 μm PES membrane. All stretching performed at 160°C and a strain rate of 0.1 cm/s.

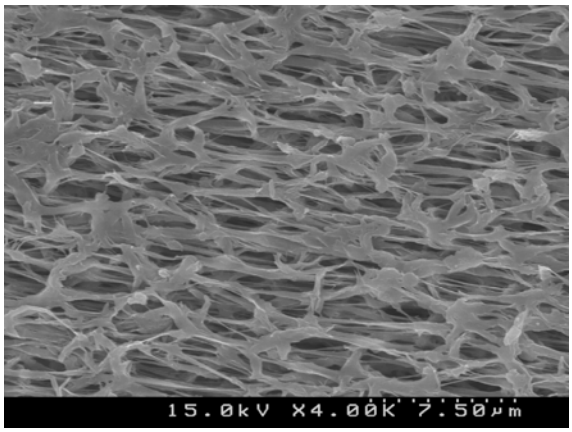

100% Stretch Aspect Ratio = 4.4

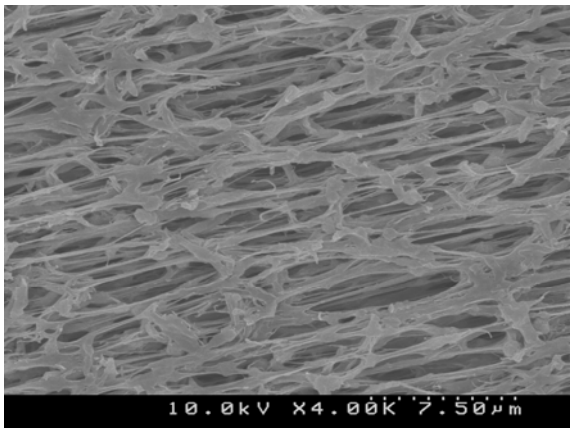

150% Stretch Aspect Ratio = 4.6

Figure 22: Pictures of ~0.2 mm PES membrane shown at both 100% and 150 % total strain to demonstrate the change in aspect ratio. All stretching performed at 160°C and a strain rate of 0.1 cm/s.

The porosity of the membrane is a reflection of how much void space the membrane contains. The procedure for measuring the porosity is given above. The average porosity for the membrane increases with stretching as shown in Figure 23. This result is expected because as the membrane is stretched the pores become larger and there is less polymer per unit volume. This result could lead to a weakening of the membrane because of the loss of density of the membrane. It will be important in the future to determine whether or not the combination of both thinning of the membrane and the increase in porosity yields a membrane that can not stand the forces of back flushing and high pressure filtration.

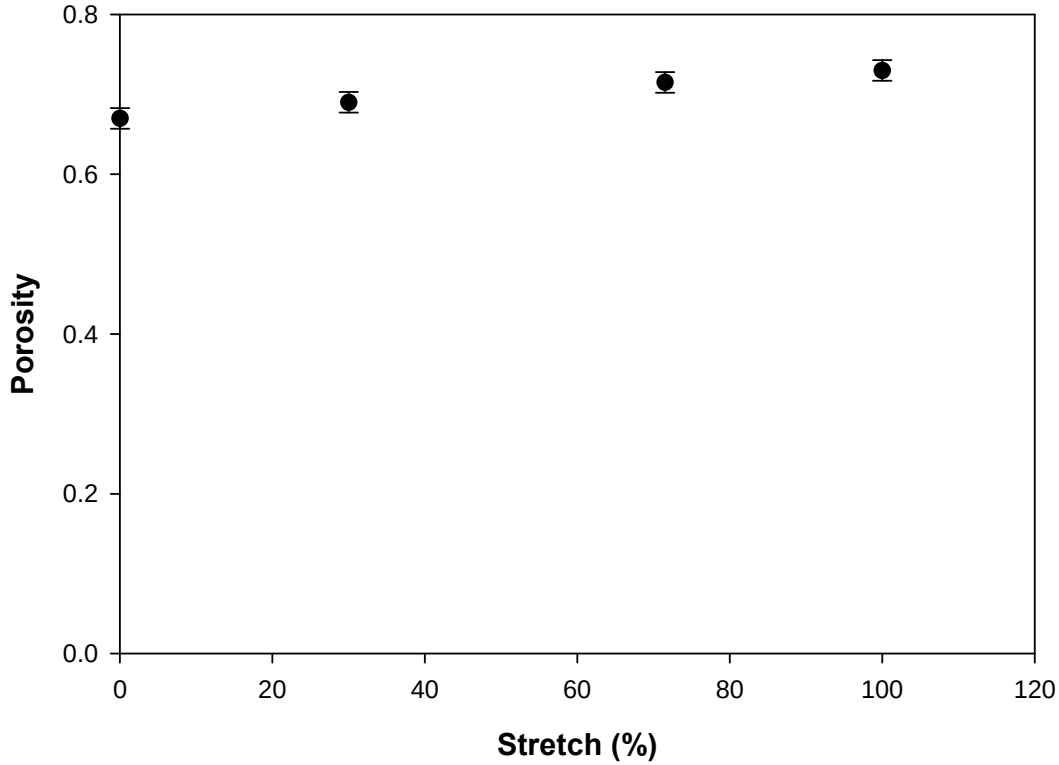

Figure 23: Effect of stretching on membrane porosity for ~0.2 μm PES membranes. All membranes shown were stretched at 160°C and a strain rate of 0.1 cm/s.

Permeation Experiments: Flux Results

T-E Membranes: Pure Water Results

Pure water flux studies were conducted at room temperature with water cleaned by the Milli-Q system. Pure water experiments were done in tandem with particle challenge experiments, but the results are discussed separately. Pressure was adjusted for each membrane to allow for a reasonable length of experiment and then taken into account by reporting permeance rather than flux.

Pure water flux studies were performed on the PET sample with 0.6 μm pore size with stretches of 0% and 26%. Results form these studies, given in Figure 24, show excellent repeatability between samples, and they also show that stretching significantly increases permeance. The scatter evident in some of the data early in the experiment may be due to the lag time for pressure equilibrium to occur.

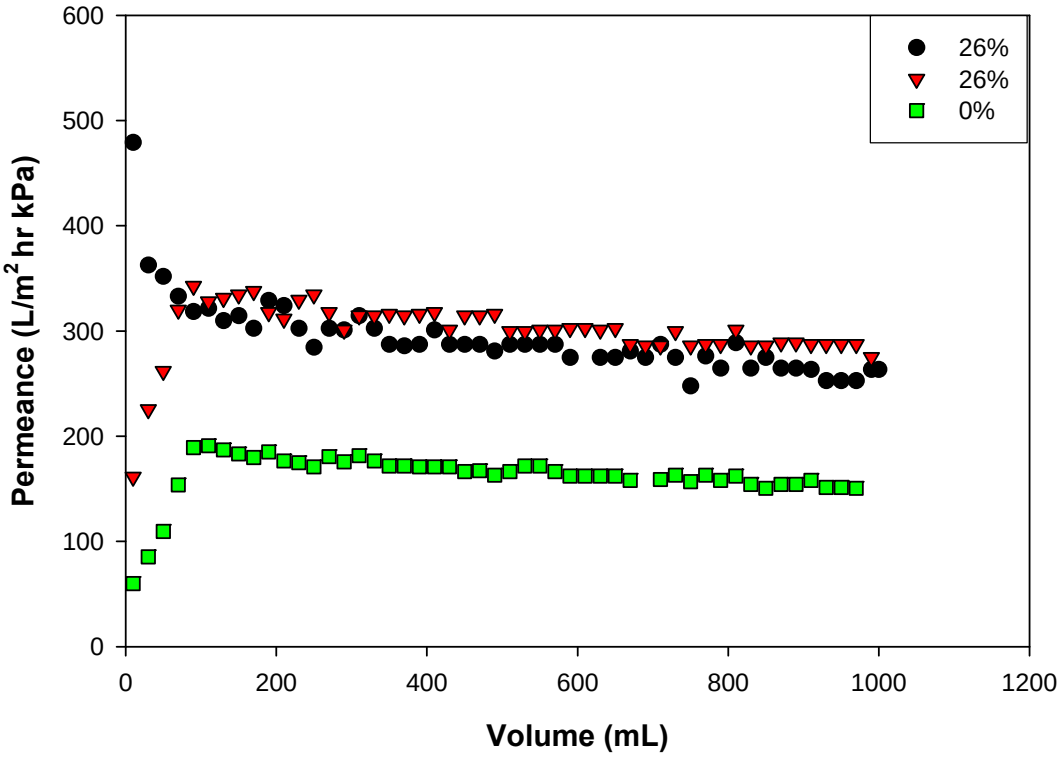

Figure 24: Effect of strain on pure water flux through 0.6 μm PET membranes.

Pure water flux studies were also performed on membranes of pore size 1, 2, 3, and 10 μm; however, results for these membranes were inconclusive. The inconsistencies in the pure water flux results could be a consequence of the inconsistencies indicated in Table 4. As mentioned when Table 4 was discussed above, additional work in the future is needed to resolve these inconsistencies.

T-E Membranes: Min-u-sil Particle Challenge Studies

Min-u-sil 5 was used as particulate challenge for PET membranes with pore sizes of 1, 2, and 3 μm. All studies were conducted at room temperature, and pressure was adjusted for each membrane to allow for a reasonable duration of experiment. All studies were conducted at a particle concentration of 10 mg/L. The module was not stirred, but the reservoir was stirred to keep suspension concentration uniform throughout the experiment.

Figure 25 shows the results from particle challenge experiments performed on 0 and 12% stretched 1 μm PET membranes. Approximately 9.9% of the particles in Min-u-sil 5 are smaller than 1 μm in diameter. This figure again demonstrates the high repeatability obtained between samples and experiments. The results show that stretching increases permeance and decreases flux decline for feed solutions containing Min-u-sil particles. The data were further analyzed using a Hermia analysis, which characterizes fouling for pressure driven flow through a membrane. The Hermia analysis is completed by using Equation 6 to linearize flux data.

$$\frac{d^2t}{dV} = k\left(\frac{dt}{dV}\right)^n \qquad (6)$$

If flux data is linearized by setting *n* equal to one and plotting time/volume versus volume then the filtration is controlled by a cake building up on the surface according to Hermia analysis. Figure 26 shows the Hermia analysis for the 1 μm PET with 10 mg/L Min-u-sil 5 suspension feed. The stretched membrane shows lower resistance to flux (that is, lower slope). The Hermia analysis was only applied to the linear portion of the plots, which correspond to constant pressure operation; the fact that the pressure in these experiments varied at the beginning of the experiments caused the curvature in Figure 26. The experiments for the other PET membranes required constant adjustment of the pressure; thus, no Hermia analysis is presented for the other PET Membranes.

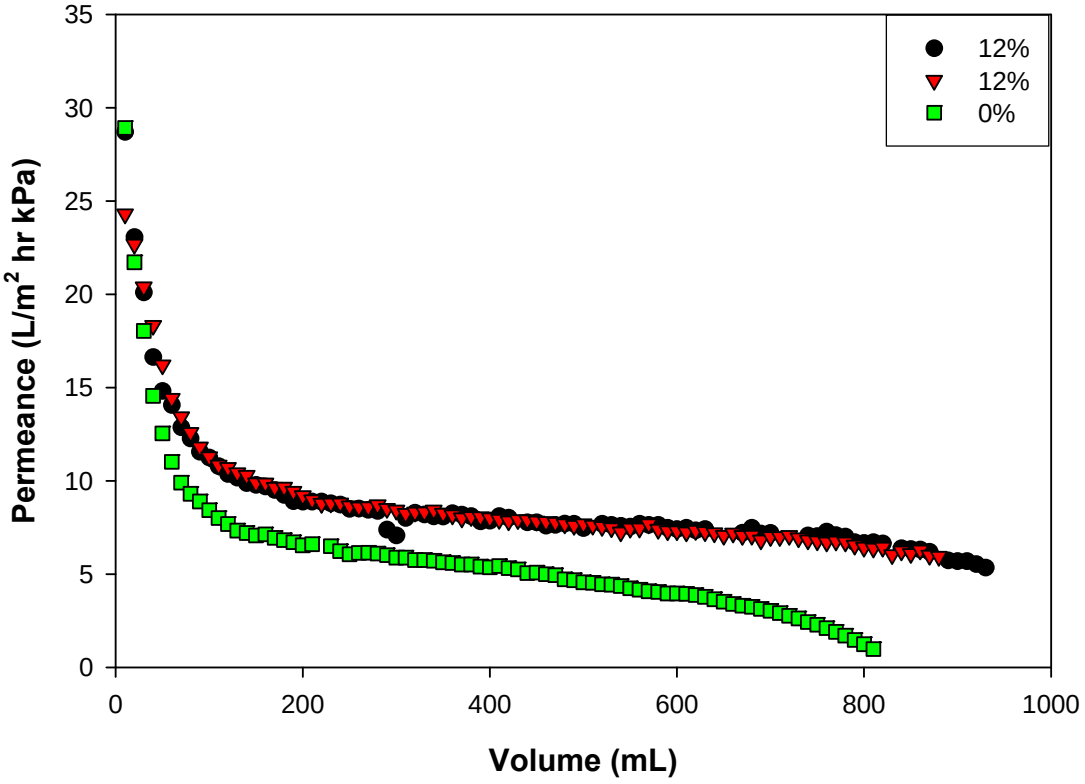

Figure 25: Effect of strain on permeance as a function of permeate volume for 1 μm PET membrane. Min-u-sil 5 fed at 10 mg/L.

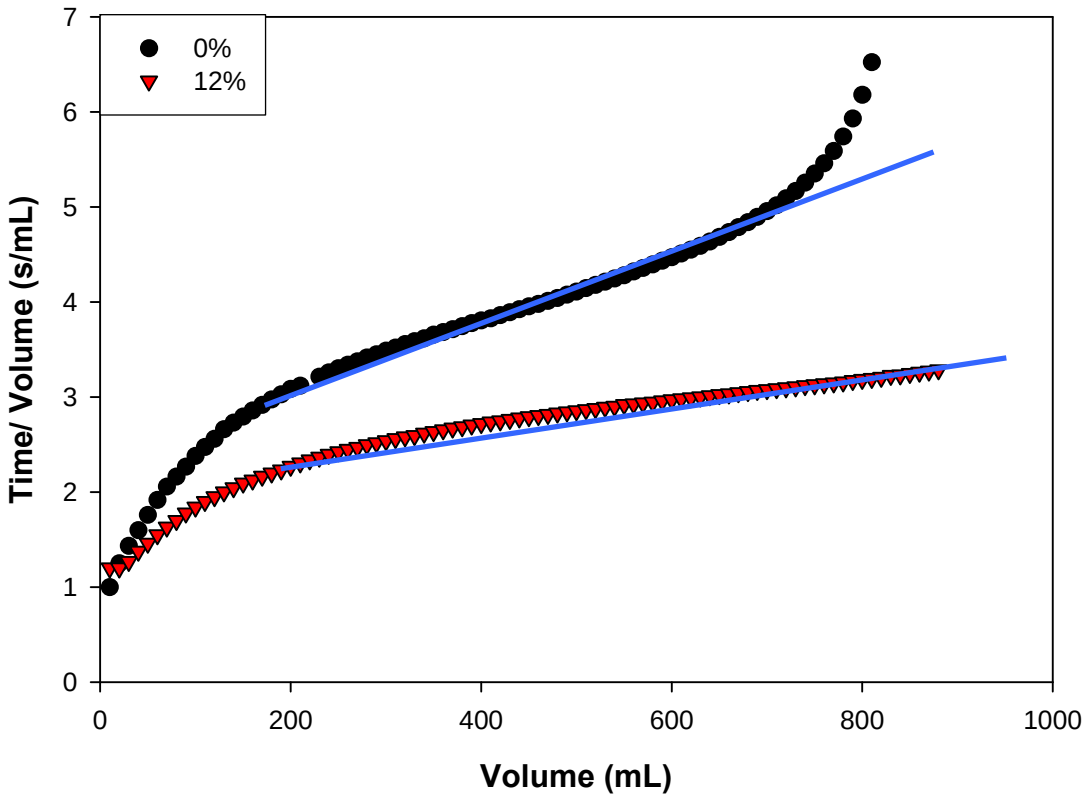

Figure 26: Hermia analysis for 1 μm PET. Min-u-sil 5 fed at 10 mg/L.

Results from the 2 μm PET studies, shown in Figure 27 for a variety of stretches, also show that stretching increases flux and decreases flux decline for particulate challenge experiments. Approximately 26% of the particles in Min-u-sil 5 are smaller than 2 μm. The 3 μm PET samples did not show a significant increase in permeance with stretching, as shown in Figure 28. Approximately 43% of the particles in Min-u-sil 5 are smaller than 3 μm.

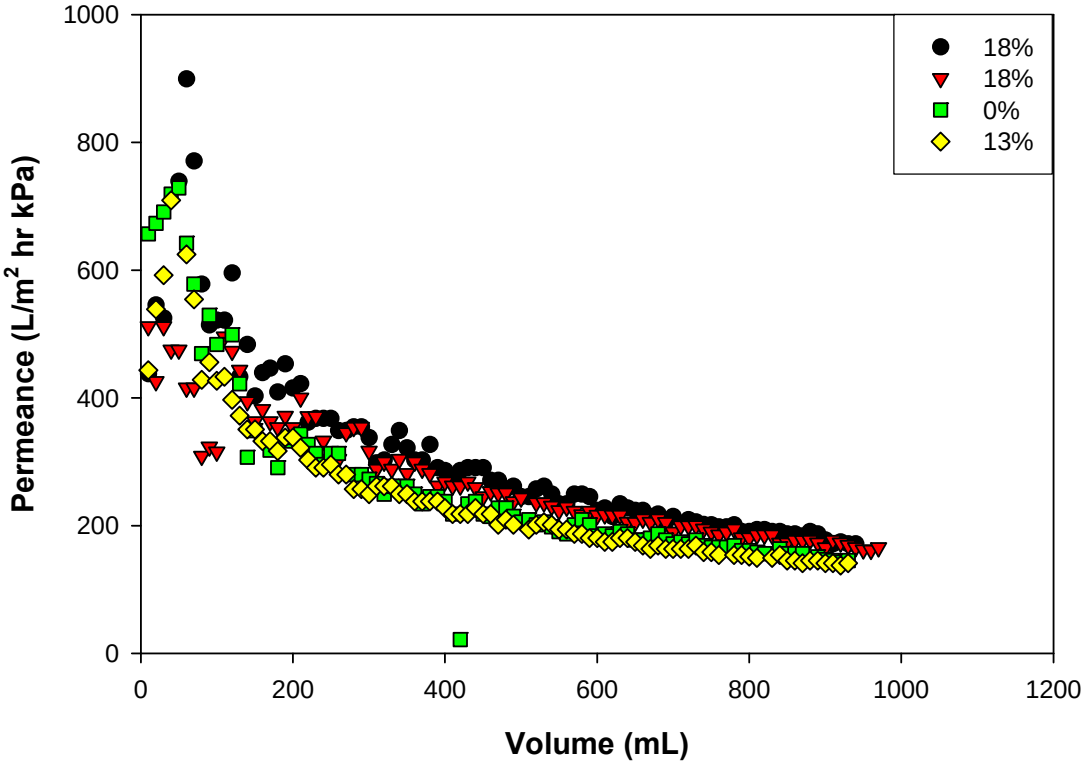

Figure 28: Effect of strain on permeance as a function of permeate volume for 3 μm PET membranes. Min-u-sil 5 fed at 10 mg/L.

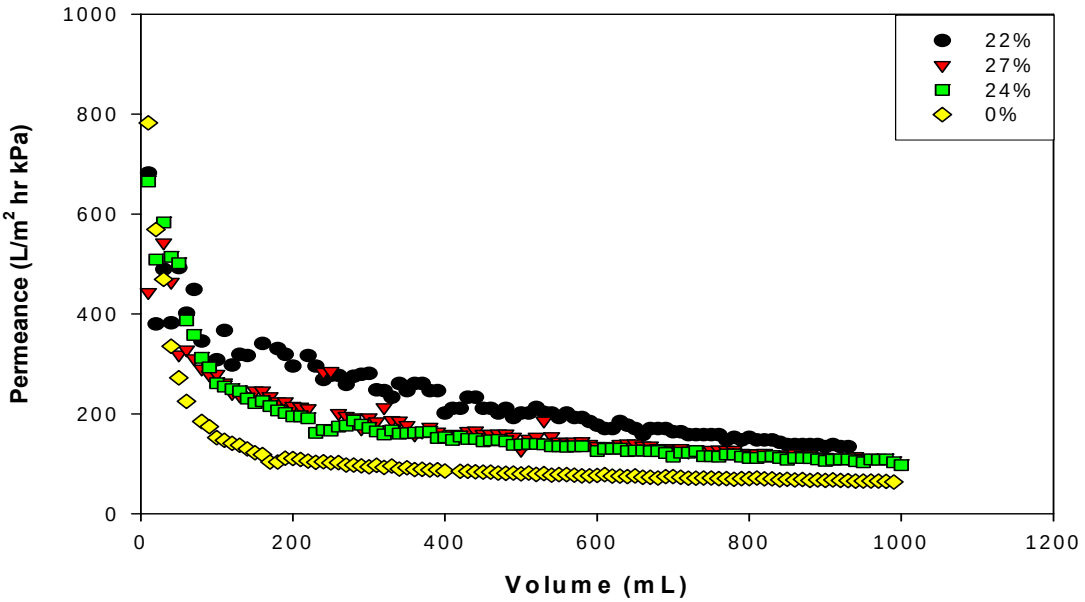

Figure 27: Effect of strain on permeance as a function of permeate volume for 2 μm PET membranes. Min-u-sil 5 fed at 10 mg/L.

Min-u-sil 30 was used for the 10 μm PET samples. The suspension concentration was 10 mg/L, and experiments were performed in the same way as the previously described Min-u-sil 5 experiments. There was some increase in permeance for samples stretched 14 and 18%. This

sample had a very high flux, making volume readings difficult, which caused some scatter for the first 200 mL of the experiment, as shown in Figure 29.

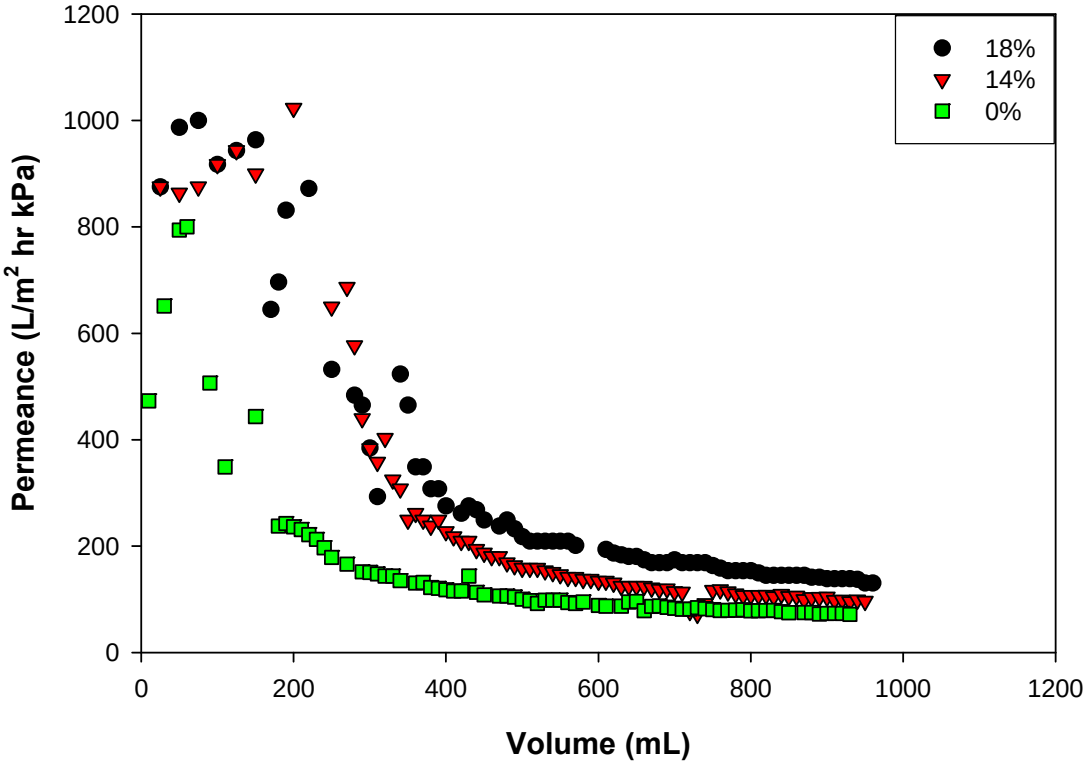

Figure 29: Effect of strain on permeance as a function of permeate volume for 10 μm PET membranes. Min-u-sil 30 fed at 10 mg/L.

In summary, the challenge studies with irregular shaped particle suspensions fed to track-etched PET membranes indicates that stretching has the potential of reducing flux decline. Decreased flux decline could have positive financial impact on membrane applications by decreasing the frequency of stopping the process for back-flushing to clean the membranes. While further work is needed to quantify the effect of stretching on flux decline and to see if the frequency of back-flushing can be reduced, the results are encouraging enough that additional financial support was garnered from other agencies to continue this study.

T-E Membranes: Spherical Beads Challenge Studies

Spherical polystyrene beads with nominal diameter 0.652 μm from Duke Scientific Corporation were used for particle challenge studies for the 0.6 μm PET membranes. Suspensions at concentrations of 10 mg/L were used, and experiments were conducted at room temperature with an unstirred module and stirred reservoir. Results, shown in Figure 30, show that there is an increase in permeance for 26% stretched samples, but the difference in performance decreases as more fluid passes through the membrane and the layer of rejected beads accumulates.

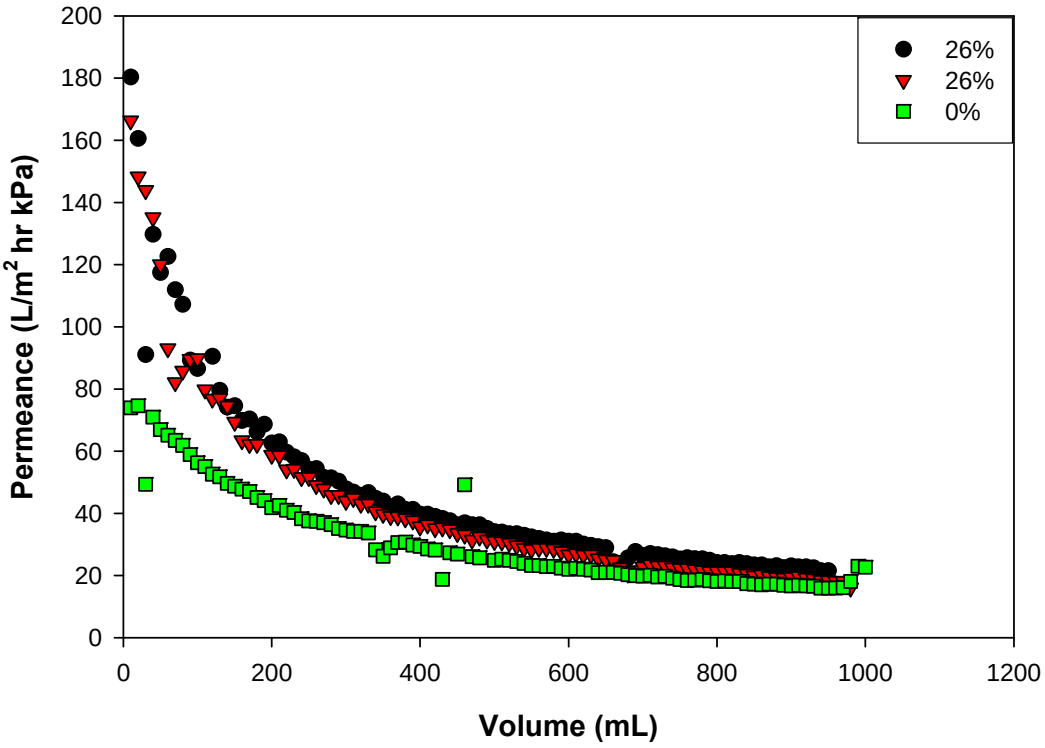

Figure 30: Effect of strain on permeance as a function of permeate volume for 0.6 μm PET membranes. 0.625 microsphere suspension fed at 10 mg/L.

Spherical beads of diameter 2.02 μm were used as particle challenge for the 2 μm PET membrane. Results, given in Figure 31, show a significant increase in flux for samples stretched 22, 24, and 27%. Again, the difference in performance decreases as more fluid passes through the membrane and the layer of rejected particles accumulates.

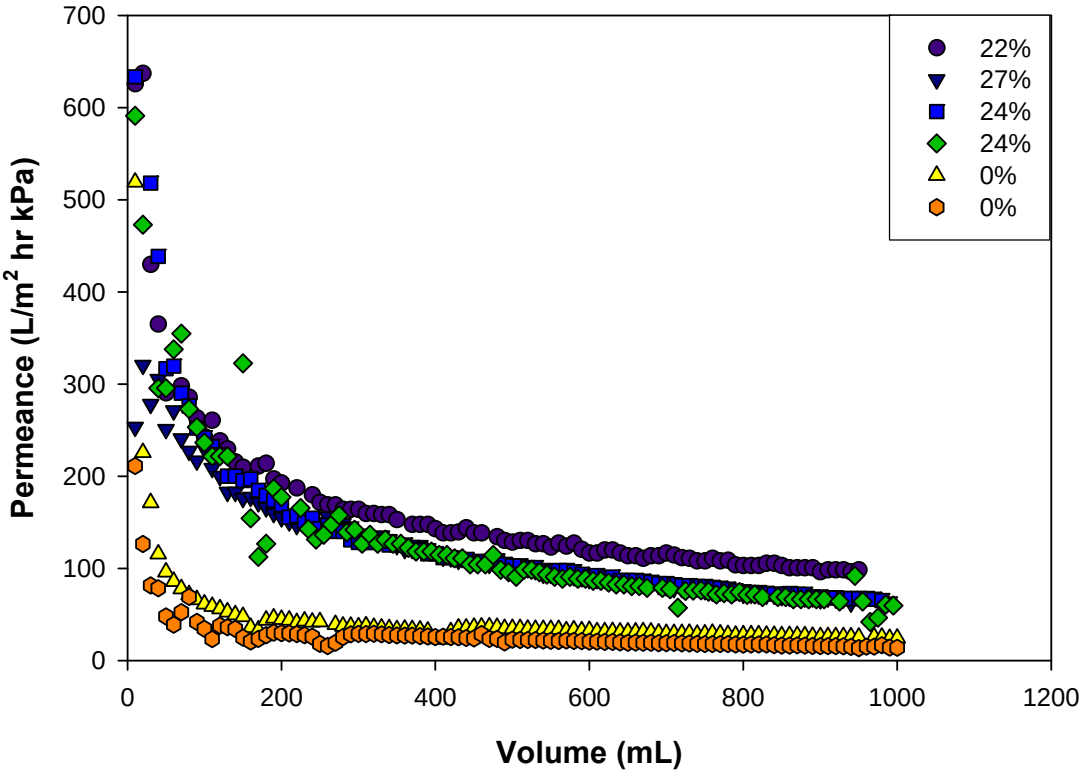

Figure 31: Effect of strain on permeance as a function of permeate volume for 2 μm PET membranes. 2.02 μm microsphere suspension fed at 10 mg/L.

The results presented in Figures 25 to 31 for the particle challenge studies (with irregular shaped particles as well as spheres) are encouraging. The rate at which the permeance declines is reduced by stretching the membranes. In practice this means that back-flushing of the membrane to remove accumulated particulate layers can be carried out less frequently, thereby realizing significant economic benefit.

PI/PS Membranes: Pure Water Results

Pure water flux studies were conducted at room temperature with water cleaned by the Milli-Q system. Pure water experiments were done in tandem with particle challenge experiments, but the results are discussed separately. All experiments were done at 20 psig pressure. Permeance through the membrane was adjusted with respect to membrane thickness so that membranes of various levels of stretching could be compared in terms of performance. This adjustment was done by multiplying the measured permeance by the membrane thickness. Multiplication is done because flux through a membrane is inversely proportional to membrane thickness; that is, as membrane thickness goes down flux increases.

Data for the pure water experiments with the ~0.2 μm PES membrane is shown in Figure 32. Initial variation in the data is due to pressure equalization in the system over the first 100 - 150 mL of flux. There appears to be a significant increase in flux between a non-stretched membrane and a membrane with a 14% strain. However, no significant increase or decrease in

flux is evident above 14% strain. Future work will be directed at the study of very low strains on membrane performance.

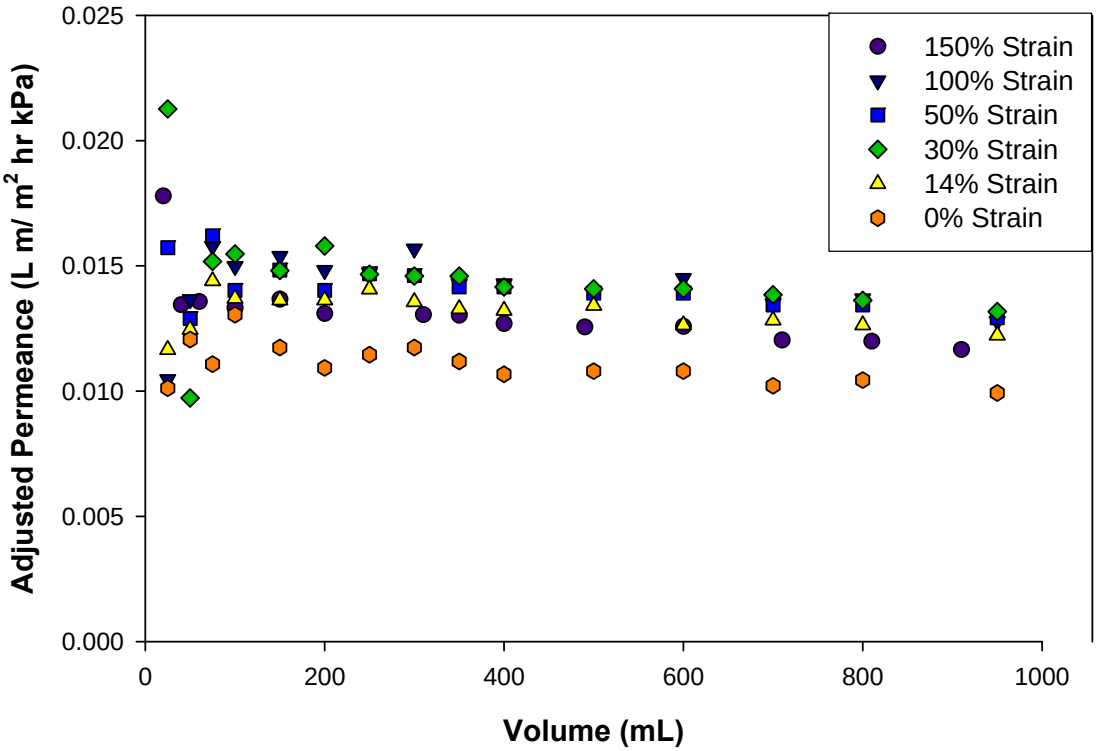

Figure 32: Effect of strain on pure water permance as a function of permeate volume for ~0.2 μm PES membranes. Permeance is adjusted for membrane thickness.

PI/PS Membranes: Min-u-sil Particle Challenge Studies

Min-u-sil 5 consists of irregular shaped particles with a broad size distribution as shown in the previous section. It was used in initial experiments to validate the methodologies of experimentation and analysis of the data collected. The results of these particle challenge studies are shown in Figure 33. The data shown in Figure 33 represent the flux normalized to the pure water flux for each membrane. This normalization was done by dividing the solution flux dividing by the estimated initial flux (obtained by extrapolating the adjusted flux back to zero permeate volume). The flux and flux decline for non-stretched and stretched membranes appears to be the same.

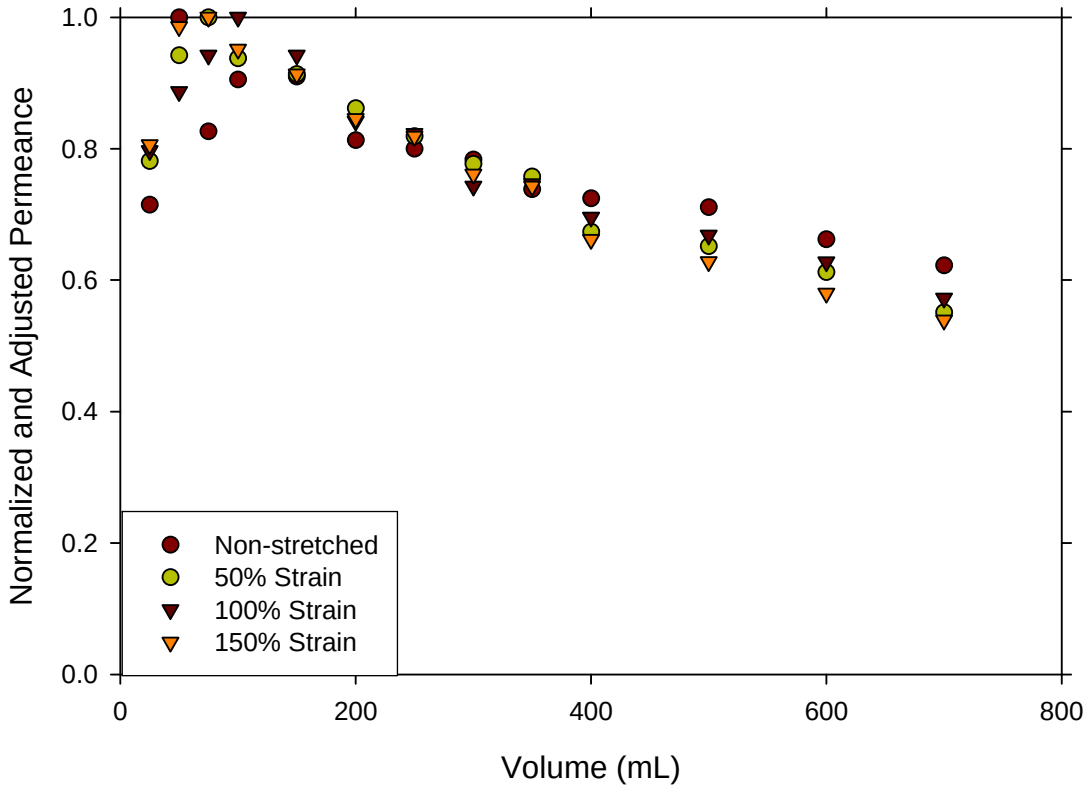

Figure 33: Effect of strain on permeance as a function of permeate volume. ~0.2 mm PES membrane. Experiment performed at 20 kPa with a Min-u-sil 5 suspension fed at 50 mg/L. Permeance is adjusted for membrane thickness.

Figure 34 is a plot of the Hermia analysis using Min-u-sil 5 at a concentration of 50 mg/L in the suspension. The linear form of the data shows that the flow through the membrane is controlled by the filter cake on the surface. This result is expected because of the large particle size of the Min-u-sil. In flux experiments Min-u-sil quickly builds up on the surface of the membrane and once the cake forms the membrane is nothing more than a porous support. In Hermia analysis the slope of the line reflects the rejection of particles by the membrane with a small slope being interpreted as low rejection. By this analysis the slope of the non-stretched and the 50% and 100% stretches are approximately equal. The 150% stretch membrane shows a slope of almost zero, which can be interpreted as a decreased rejection due to stretching.

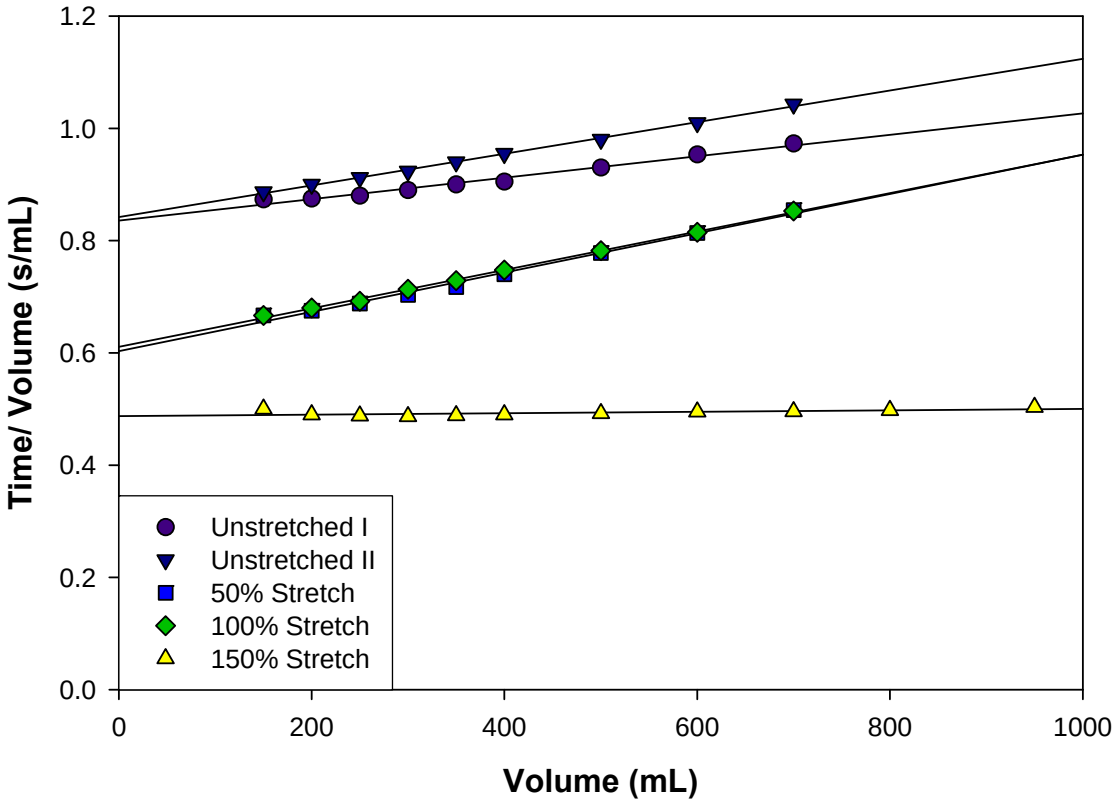

Figure 34: Hermia analysis shown for ~0.2 μm PES membrane to demonstrate the change in rejection upon stretching with a feed of 50 mg/L Min-u-sil 5 suspension.

PI/PS Membranes: Spherical Beads Challenge Studies

Cross linked polystyrene beads of an average particle size of 0.17 μm were used for testing with the ~0.2 μm PES membrane. It is important to note that the pore sizes on the membrane are not equal to the rated rejection size for the membrane. For example the ~0.2 μm PES membrane is advertised to rejecting 90% of particles greater than or equal to ~0.2 μm in

diameter. According to results from digital image analysis of surface pore characteristics, the pores in the ~0.2 µm PES membrane are actually significantly larger than 0.2 µm, meaning the 0.17 µm particles were of a significantly smaller diameter than that of the pores on the membrane. The flux and flux decline through the membrane, as given in Figure 35, show no discernible difference between the non-stretched and the stretched membranes. The data shows that little or no gain was achieved in either membrane flux or flux decline by stretching the membrane for this particular feed.

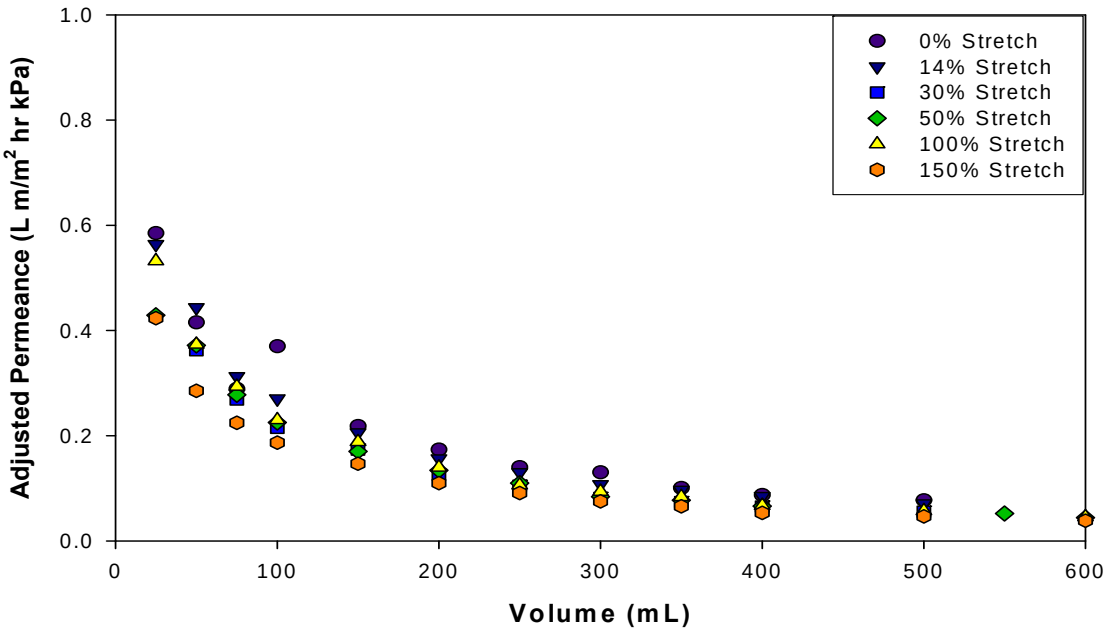

Figure 35: Effect of strain on permeance as a function of permeate volume. ~0.2 mm PES membrane. 0.17 µm microsphere suspension fed at 10 mg/L. Permeance is adjusted for membrane thickness.

This data was also analyzed using the Hermia analysis and the results shown in Figure 36 indicate that the flow through the membrane with the micro spheres is controlled by a cake building on the surface of the membrane. SEM analysis of the membranes cross section after filtration verified these results by revealing a cake of particles on the surface. Some beads are found trapped within the bulk of the membrane but most are found on the surface. It is not immediately clear why no beads are found within the membrane bulk. Possible reasons to explain the lack of penetration are that samples were prepared for SEM by breaking the membrane in liquid nitrogen, which could have washed away any particles trapped in the membrane. A surface charge on the membrane or between particles could have caused the particles to build up on the surface and not penetrate the membrane or a flow pattern in the water over the membrane could have developed and prevented the particles from entering into the porous structure. Further research is required to understand fully why the 0.17 µm polystyrene spheres did not penetrate the surface of the membrane.

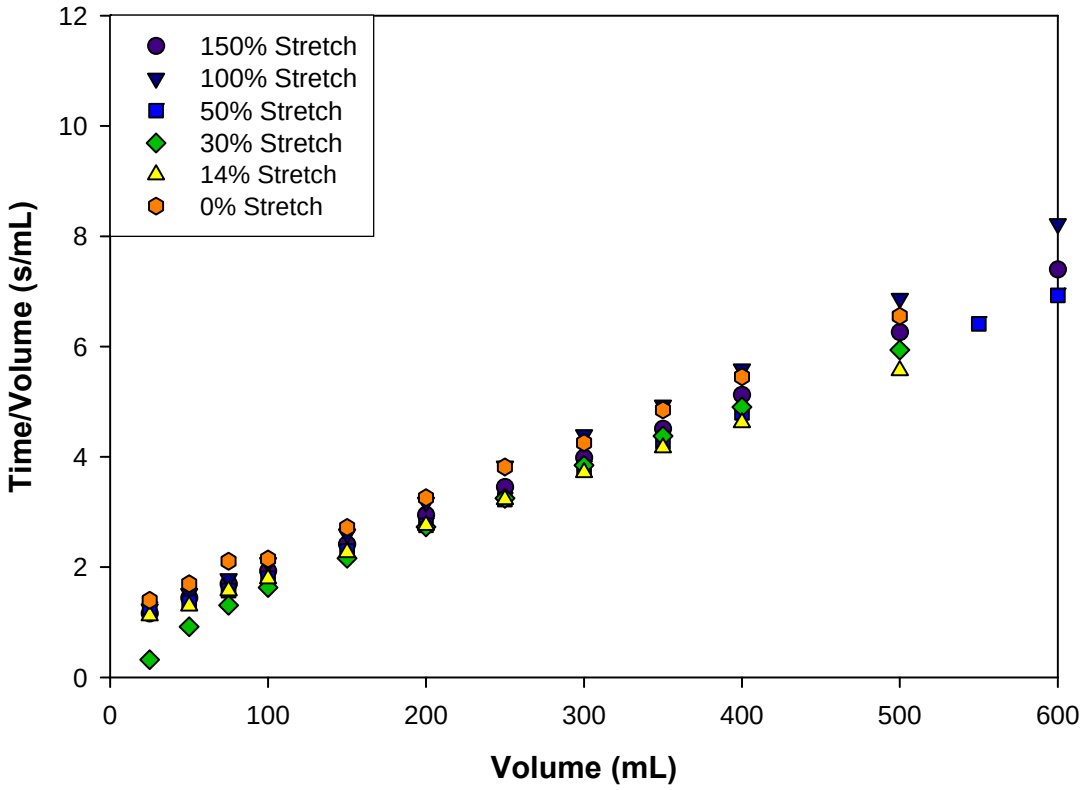

Figure 36: Hermia analysis for ~0.2 μm PES membrane. 0.17 μm microsphere suspension fed at 10 mg/L.

Permeate samples were taken in the microsphere experiments and turbidity was measured for those samples. The turbidity data given in Figure 37 shows that the majority of particles did not make it through the membrane, which is in agreement with the findings reported in the previous paragraph. The turbidity of the unfiltered solution was approximately 42 ± 0.1 which means that more than 99.9% of the polystyrene microspheres were rejected by the membrane after only 200 mL of flow no matter what the degree of strain. Some particles did pass through the membrane in the initial 100 – 200 mL of the experiment but the membrane quickly fouled and prevented more particles from passing through.

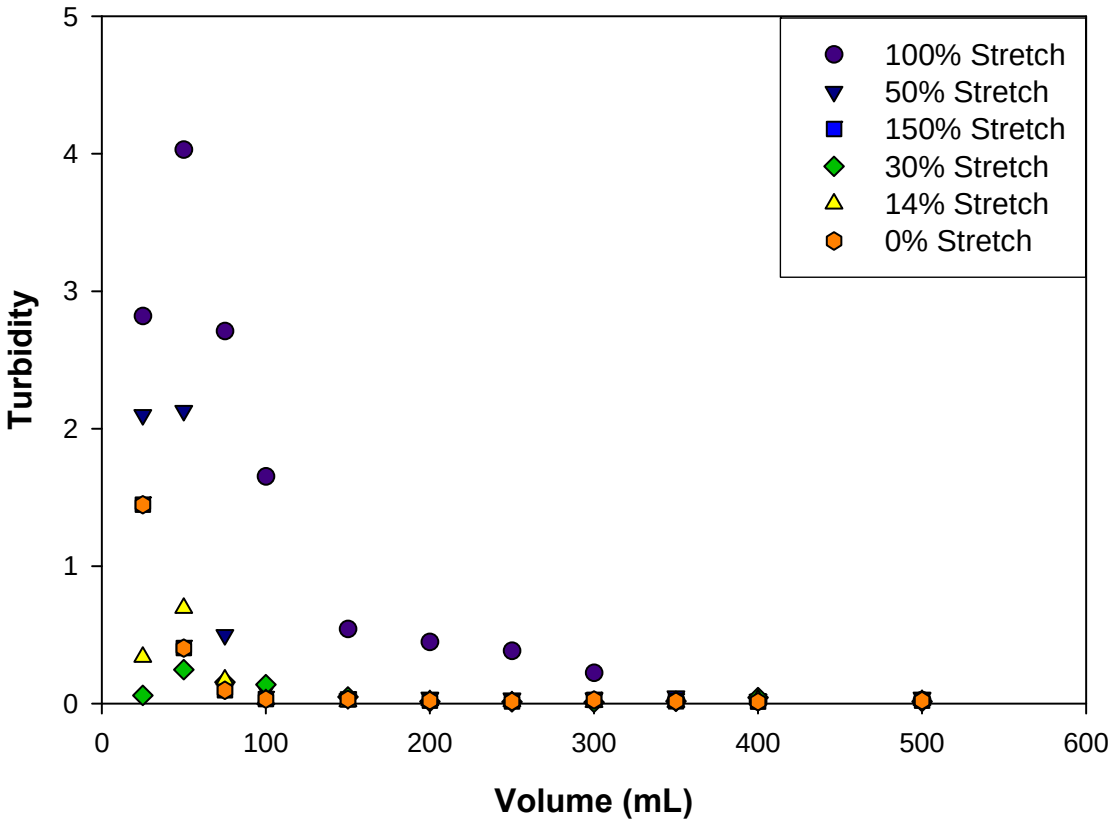

Figure 37: Effect of strain on turbidity of permeate. ~0.2 μm PES membrane. 0.17 μm microsphere suspension fed at 10 mg/L.

PI/PS Membranes: Protein Fouling Studies

A 1 g/L bovine serum albumin (BSA) phosphate-buffered solution (pH=7.4) was used as the model for protein fouling of 0.2 μm poly(ether sulfone) phase inversion membranes. Experiments were performed in dead-end filtration at room temperature (T= 22°C).

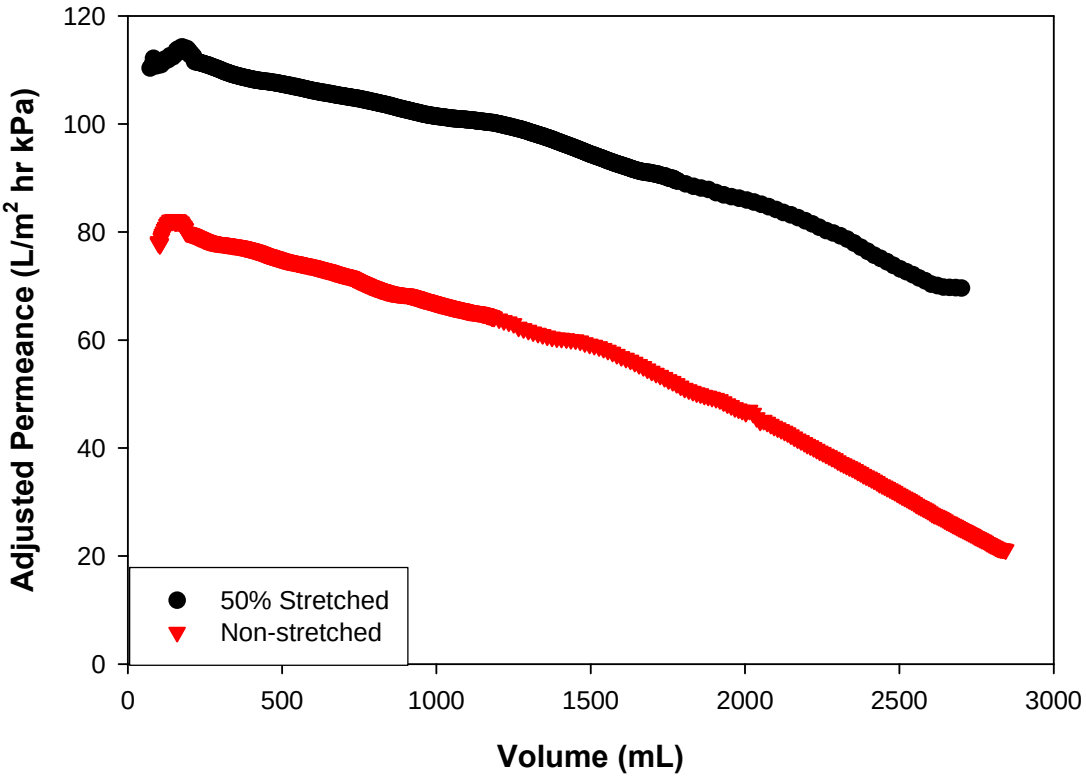

Figure 38: Adjusted permeance for stretched and non-stretched 0.2 mm PES in dead end filtration. 1 g/L BSA. Permeance is adjusted for membrane thickness.

Figure 38 shows that the flux of the membrane was significantly increased by stretching the membrane by 50% (companion data not reported here indicated that the rejection of the BSA was not changed by stretching.) The fact that flux decline was improved by stretching is not immediately evident in Figure 38; however, when the data are "normalized" by dividing solution flux by the estimated initial flux (obtained by extrapolating the lines in Figure 38 back to zero volume) and plotted as shown in Figure 39 it becomes evident that stretched membrane has a slower flux decline than the non-stretched membrane. Again, the significance of a slower flux decline is that back-flushing will be required less frequently; thereby reducing costly losses in productivity.

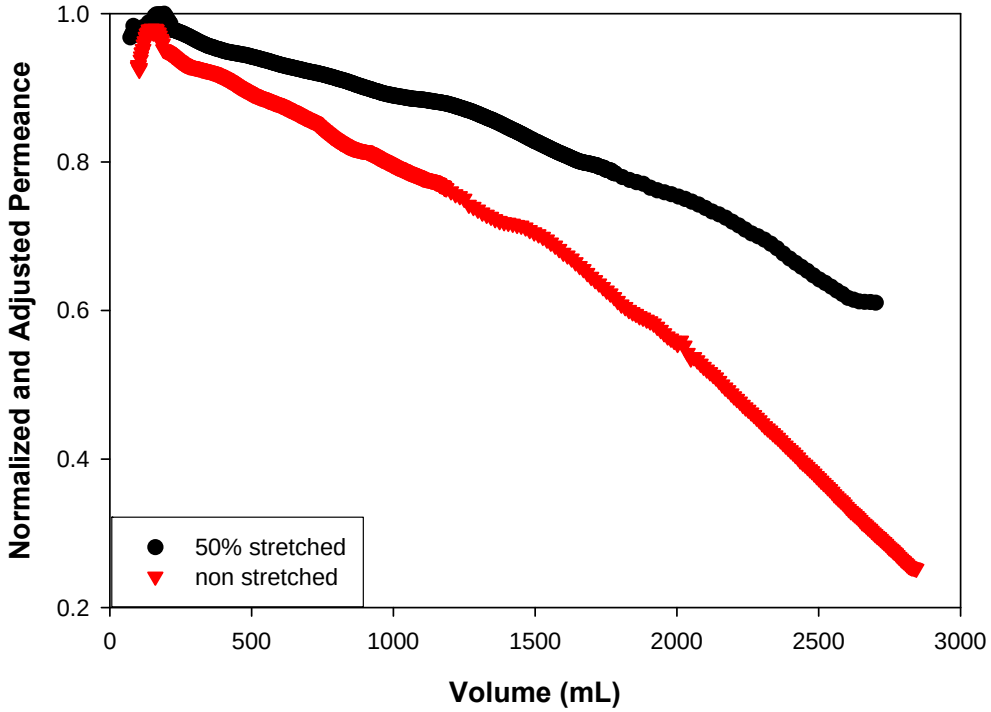

Figure 39: Normalized and adjusted permeance for stretched and non-stretched ~ 0.2 μm PES with 1 g/L BSA feed solution. Permeance is adjusted for memrane thickness.

Figure 40 is included in this report because it provides the reader with an interesting insight into the value of plotting data against permeate volume rather than operating time. Much of the published literature report data as a function of time; however, the important factor influencing flux decline is not the length of time the membrane has been in operation, the important factor is how much permeate has passed through the membrane and consequently how much rejected material has built up on the surface of the membrane or within the bulk of the membrane. Thus, Figure 40 would indicate that stretching does not influence flux decline, while in reality stretching does decrease flux decline as Figure 38 clearly shows.

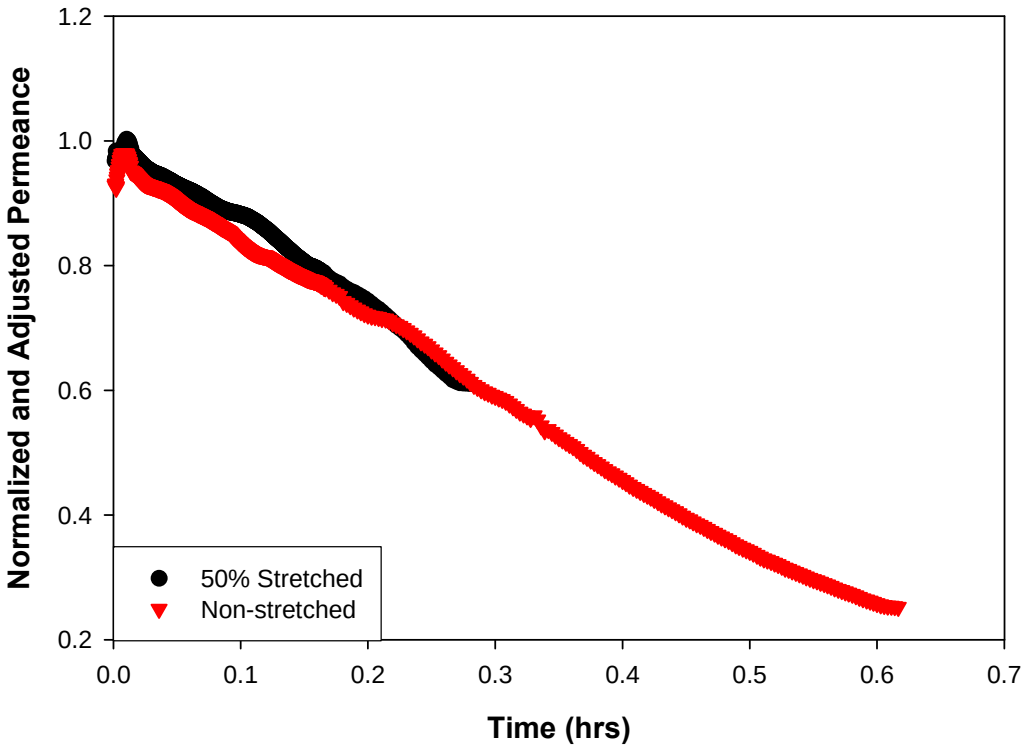

Figure 40: Normalized and adjusted permeance for stretched and non-stretched ~ 0.2 mm PES with 1 g/L BSA feed solution. Permeance is adjusted for membrane thickness.

Permeate Analysis and Rejection Results

T-E Membranes: Min-u-sil Particle Challenge Studies

Particle challenge experiments were performed using Min-u-sil 5 for 1 μm, 2 μm, and 3 μm track-etched membranes and using Min-u-sil 30 for 10 μm track-etched membranes. Samples were collected throughout each experiment so that the particle rejection capability of each membrane could be examined over time and compared for different volume throughputs. Samples were analyzed using the Coulter Counter, and the resulting data were used to plot particle size distribution functions (PSDF) versus the log of the equivalent spherical particle diameter. The PSDF is the number concentration of particles in a small size increment, normalized by dividing by that size increment. The normalization means that the results should be independent of the instrument, laboratory, and operator. Channels represent a narrow size range that the Coulter Counter groups together when it counts particles. The log scale on the ordinate of the particle size distribution function means that for the data presented, a decrease of one represents an order of magnitude loss in the number of particles. Therefore, if there was an average difference of two between the particle size distribution function for the original feed suspension and that for a permeate sample, there would be 2 log removal of particles or 99% removal.

Experimental results for 1 μm PET membranes, presented in Figures 41 and 42, show that the membranes, stretched and non-stretched, achieve anywhere from 2 to 3 log removal of

particles when compared with the feed suspension, and this removal generally improves over time. Figure 41 is a PSDF for a non-stretched membrane showing improvement in rejection over time. A comparison of the PSDF for a 12% stretched 1 μm PET membrane to non-stretched membranes, shown in Figure 42, indicates that stretching the membrane may (slightly) improve particle rejection. The results for different sets of samples for the non-stretched membranes do not compare well however, indicating the particle rejection data are not exactly repeatable. Therefore, the results should be regarded as preliminary and the experimental procedure may have to be improved to ensure the highest quality data; the Coulter Counter requires scrupulous care to ensure repeatability.

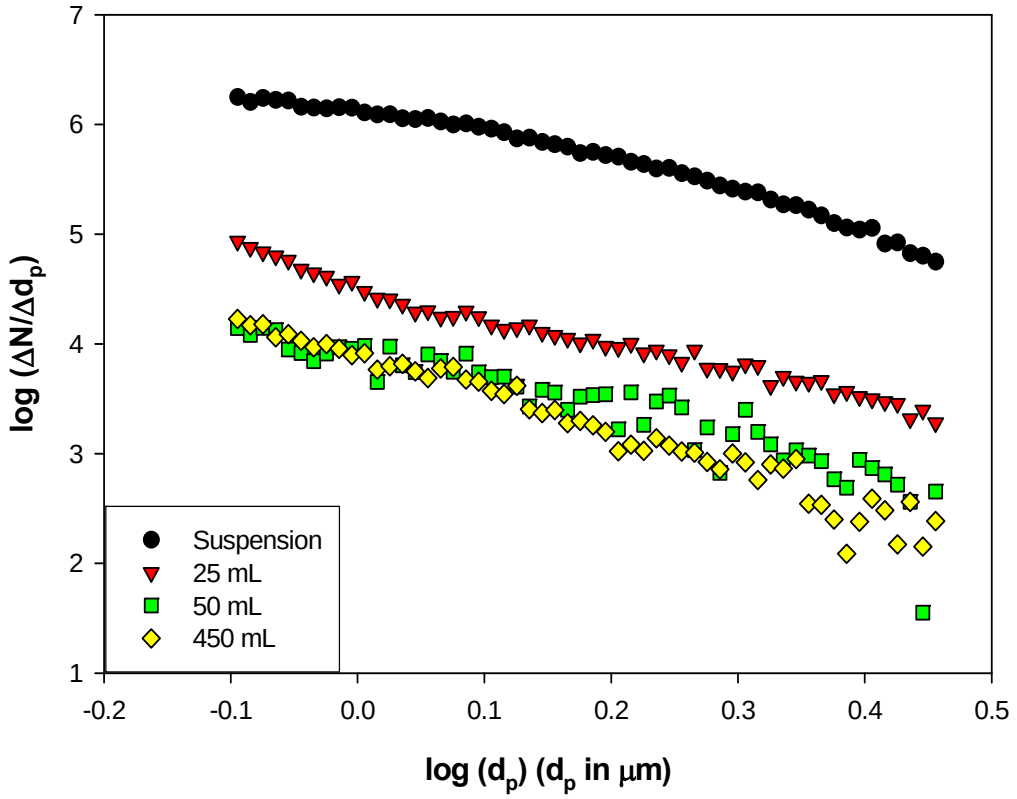

Figure 41: PSDF for non-stretched 1 mm PET with a feed of 10 mg/L Min-u-sil 5.

Figure 43 shows some of the results for the Min-u-sil 5 particle challenges using 2 μm PET membranes. In comparison to the 1 μm PET membranes, the removal in these 2 μm PET membranes is not as great, as one might expect with the larger pore sizes. Counts for particles greater than 2 μm in diameter (log $d_p > 0.3$) may be too low to be statistically significant. For particles smaller than 2 μm, the PSDFs indicate that stretching the membranes does not result in significant improvements in particle rejection.

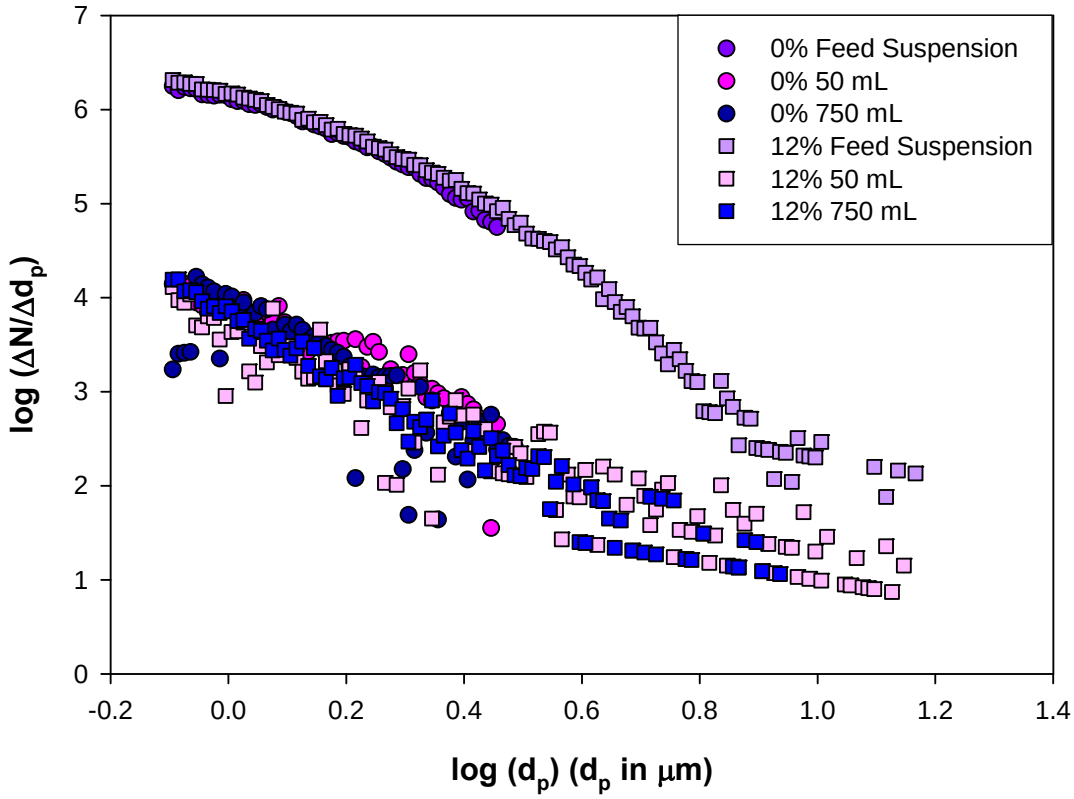

Figure 42: PSDF for 1 μm PET with a feed of 10 mg/L Min-u-sil 5.

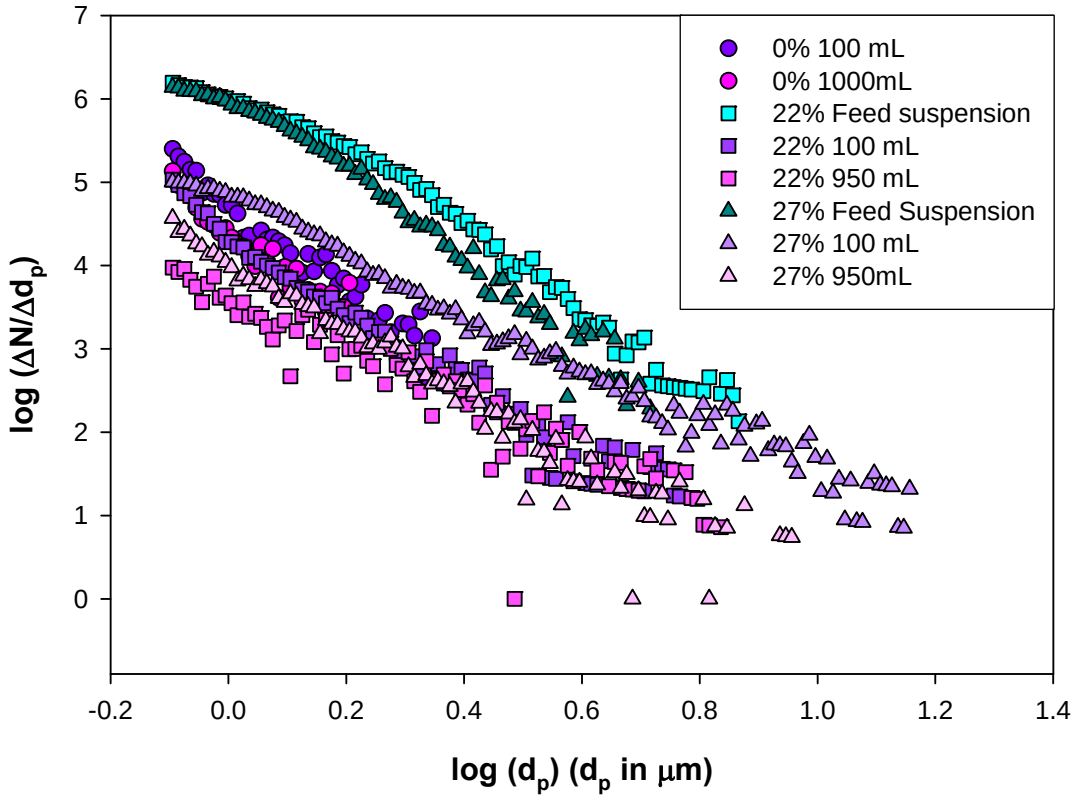

Figure 43: PSDF for 2 μm PET with a feed of 10 mg/L Min-u-sil 5.

Coulter Counter analysis results for Min-u-sil 5 particle challenges using 3 μm PET membranes seemed repeatable for samples at some volume throughputs and not repeatable at others. Table 5 presents some of these data; negative numbers in this table mean that the stretched membrane achieved better removal the non-stretched membrane. The results from the membrane stretched 13% are virtually all positive, meaning that, after stretching, more particles passed through the membrane. The 18% stretch apparently improved rejection of particles

Table 5: Change in number concentration for 3 μm PET with 10 mg/L Min-u-sil 5 feed.

% Difference, Particle Number Concentration (Number Concentration in #Particles/mL)					
Strain	**Volume (mL)**	**20 Channels 0.8μm-1.25μm**	**20 Channels 1.9μm-3μm**	**20 Channels 2.4μm-3.8μm**	**20 Channels 3.5μm-5.4μm**
13%	25	-19%	193%	138%	70%
18% Set 1	25	-36%	-1%	6%	-3%
18% Set 2	25	-63%	-40%	-90%	-100%
13%	50	1063%	1459%	627%	20%
18% Set 1	50	419%	305%	82%	-14%
18% Set 2	50	-75%	-66%	-84%	-100%
13%	200	1030%	1064%	359%	-23%
18% Set 1	200	45%	117%	80%	-7%
18% Set 2	200	85%	146%	101%	-100%

smaller than the pore size, while a 13% stretch appears to allow more small particles to pass through the membrane. According to these overall Min-u-sil 5 results, no vast improvement in particle rejection was achieved with the stretching of 3 μm membranes. As with the 2 μm membranes, counts of particles larger than the pore size were too small to be significant. Results were difficult to repeat, which is evident from the two sets of data for the 18% strain sample. Further study will be required to determine the effect of stretching on rejection of the 3 μm PET membrane.

For the 10 μm PET membranes, Min-u-sil 30 particle challenge samples were analyzed using two different size aperture tubes on the Coulter Counter. Use of two aperture tubes, which have accuracy over different size ranges, allowed for collection of data over a broader range of particle sizes. Overlap of the distributions in the middle range of particle sizes indicates that measurements were precise. Sample data from each of the tubes were combined and are presented together on plots of particle size distribution functions. As shown in Figure 44, data indicate that initially, for particles less than the pore size, rejection is similar for all membranes tested. As volume throughput increases, particle rejection becomes greater for the non-stretched membranes. All membranes seem to show significant rejection of particles greater than the pore size. More interesting results may be obtained by choosing particle challenge more appropriate for this pore size.

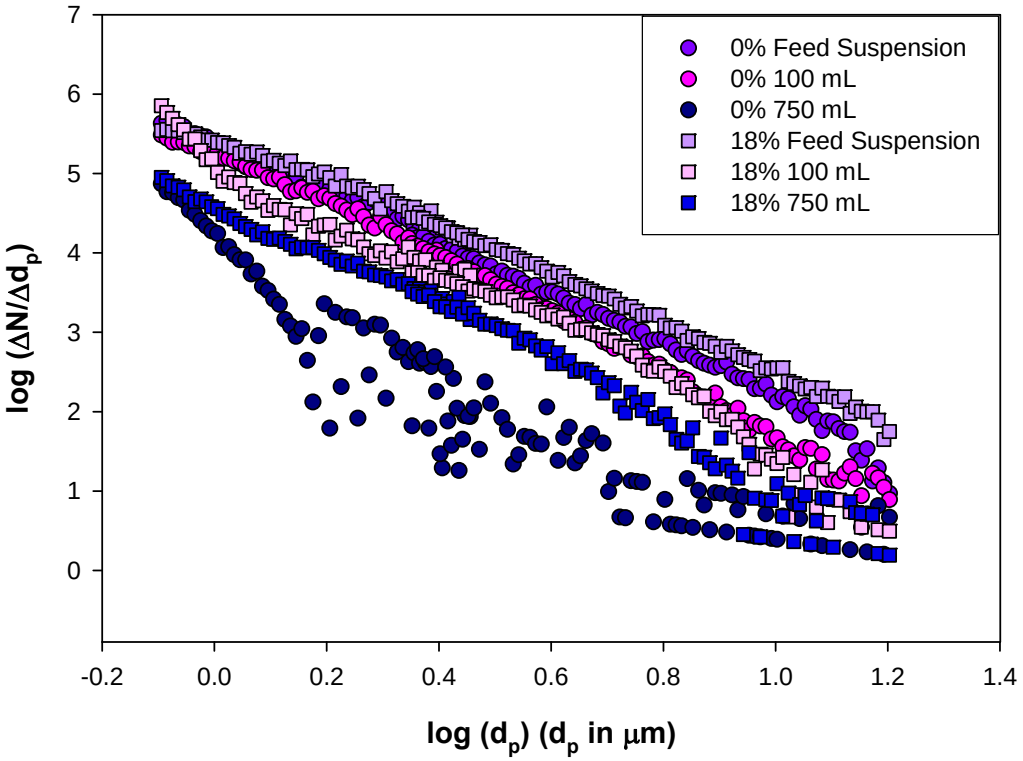

Figure 44: PSDF for 10 μm PET with 10 mg/L Min-u-sil 30 feed.

T-E Membranes: Spherical Beads Challenge Studies

Particle challenges using spherical polystyrene beads of 2.02 μm diameter were completed for the 2 μm PET membranes. Table 6 summarizes the rejection results in terms of

Table 6: Change in Number Concentration for 2 μm PET, 10 mg/L 2.02 μm Cross-linked Polystyrene Spheres.

Strain	Volume (mL)	% Difference Particle Concentration
22%	25	-65%
24%	25	-33%
27%	25	-53%
22%	50	-67%
22%	50	-74%
22%	50	-62%
22%	200	-51%
27%	200	-74%

number concentration for 22, 24, and 27% stretches compared to non-stretched membranes; as before, negative values mean that stretching improved particle removal. This presentation of the data represents the number concentration in particles per mL when data are averaged for six Coulter Counter size channels around 2 μm. Particle size distribution functions indicate some improvement in particle rejection with stretching. Greater volume throughputs do not show any significant difference between membranes because particle counts become low for all membranes. These results indicate that for the spherical particle rejection experiments, rejection improves with stretching.

CONCLUSIONS

This research has shown that it is possible to uni-axially stretch MF membranes to modify their structure. Stretching increases the major axis and decreases the minor axis of pores on the surface of both PI/PS and T-E membranes; thereby increasing the aspect ratio. Stretching also decreases the thickness of PI/PS membranes and typically increases the pore area of all membranes. These changes to membrane structure were shown in most cases to increase flux, decrease flux decline, and, in some cases, change rejection capabilities.

The results presented in this report have proven to be promising enough to attract additional funding from other sources. They are attracted by the novel approach being taken, the fundamental science being generated, and the potential for these developments to have a positive economic impact by reducing the frequency of back-flushing required in standard membrane operations.

Another benefit of the research presented here is that tailoring of the minor axis of the pores in track-etched membranes will allow the manufacturer to "created" membranes with new pore sizes. Because of the great expense involved in the manufacture of T-E membranes, these membranes are only available commercially in the sizes studies herein. Tailoring these membranes to meet the requirements satisfied by an intermediate size will lead to wider applicability of these types of membranes.

1. Ho, W.S.W. and K.K. Sirkar, eds. *Membrane Handbook*. 1st ed. 1992, van Nostrand Reinhold: New York.
2. Flemming, H.-C., G. Schaule, and R. McDonough, *How do performance parameters respond to initial miofilm formation on separation membranes?* Vom Vasser, 1993. **80**: p. 177-186.
3. Flemming, H.-C., et al., *Effects and extent to biofilm accumulation in membrane systems.*, in *Biofouling and Biocorrosion in Industrial Water Systems.*, G.G.

Geesey, Z. Lewandowski, and H.-C. Flemming, Editors. 1994, CRC Press: Boca Raton. p. 63-89.
4. Leslie, G.L., et al., *Fouling of a microfiltration membrane by two gram-negative bacteria.* Colloids and Surfaces, 1993. **A 73**: p. 165-178.
5. Wiesner, M.R.a.P.A., *Mass Transport and Permeate Flux and Fouling in Pressure-Driven Processes*. Water Treatment Membrane Processes, ed. J. Mallevialle, P.E. Pdendaal and M.R. Weisner. 1996, New York, NJ: McGraw-Hill.
6. Flemming, H.-C. and G. Schaule, *Biofouling on membranes - a microbiological approach.* Desalination, 1988. **70**: p. 95-119.
7. Ridgeway, H.F. and J. Safarik, *Biofouling on reverse osmosis membranes.*, in *Biofouling and Biocorrosion in Industrial Water Systems.*, H.-C. Flemming and G.G. Geesey, Editors. 1991, Springer: Berlin. p. 81-111.
8. Ridgeway, H.F. and H.-C. Flemming, *Membrane biofouling*, in *Water Treatment Membrane Processes.*, J. Mallevialle, P.E. Odendaal, and M.R. Wiesner, Editors. 1996, McGraw-Hill: New York. p. 6.1-6.62.
9. Hong, S.K., M. Elimelech, *Chemical and Physical Aspects of Natural Organic Matter (NOM) Fouling of Nanofiltration.* Journal of Membrane Science, 1997. **132**: p. 159-181.
10. Knoell, T., J. Safarik, T. Cormack, R. Riley, S.W. Lin, H. Ridgeway, *Biofouling potentials of microporous polysulfone membranes containing a sulfonated polyether-ethersulfone/polysulfone block copolymer: correlation of membrane surface properties with bacterial attachment.* Journal of Membrane Science, 1999. **157**: p. 117-138.
11. Hoeve, C.A.J. and M.K. O'Brien, *Specific diluent effects on polymer chain dimensions.* Journal of Polymer Science; Part A, 1963. **1**: p. 1947-1954.
12. Bierenbaum, H.S., et al., *Microporous polymeric films.* Industrial Engineering Product Research Development, 1974. **13**: p. 2-9.
13. Sarada, T. and L.C. Sawyer, *Three dimensional structure of Celgard microporous membranes.* Journal of Membrane Science, 1983. **15**: p. 97-113.
14. Kesting, R.E., *Synthetic polymeric membranes: a structural perspective*. 1985, John Wiley & Sons: New York. p. 287-310.
15. Shipman, G.H., *Microporous sheet material method of making and articles made therewith*. 1985, 3M: US.
16. Kinzer, K.E., *Method for preparing oriented microporous film*. 1993, 3M: US.
17. Kinzer, K.E., *Oriented microporous films*. 1989, 3M: US.
18. Mrozinski, J.S., *Microporous materials incorporating a nucleating agent and methods for making same*. 1988, 3M: US.
19. Mrozinski, J.S., *Multi-layer laminates of microporous film*. 1989, 3M: US.
20. Mrozinski, J.S., *Method for preparing microporous polyolefin shaped articles*. 1993: US.
21. Clinnton, P.W., *Microporous materials of ethylene-vinyl alcohol copolymer and method of making same*. 1997, 3M: US.
22. Takita, K., et al., *The preparation method for microporous polyolefin membrane*. 1991, Tonen: Japan.

23. Takita, K., et al., *Microporous polyolefin membrane and method of producing same*. 1991, Tonen Corporation: US.
24. Eshelby, J.D., *The determination of the elastic field of an ellipsoidal inclusion, and related problems.* Proceedings of the Royal Society (London), 1957. **A241**: p. 376-396.
25. Needleman, A., *Void growth in an elastic-plastic medium.* Transaction of Journal of Applied Mechanics, 1972: p. 964-970.
26. Gurson, A.L., *Continuum theory of ductile rupture by void nucleation and growth : Part 1. Yield criteria and flow rules for porous media.* Journal of Engineering Materials and Technology, Transactions of the ASME, 1977. **99**: p. 2-15.
27. McClintock, F.A., *A Criterion for Ductile Fracture by the Growth of Holes.* Journal of Applied Mechanics, 1968: p. 363-371.
28. Mohan, R. and F.W. Brust, *On Void Growth in Elastic-Nonlinear Viscous Solids Under Creep and cyclic creep conditions.* Journal of Engineering Materials and Technology, 2000. **122**(July): p. 283-293.
29. Budiansky, B., J.W. Hutchinson, S. Slutsky, *Void Growth and Collapse in Viscous Solids*, in *Mechanics of Solids*. 1982, Pergamon Press: Oxford. p. 13-45.
30. Andersson, H., *Analysis of a model for void growth and coalescence ahead of a moving crack tip.* Journal of Mechanical Physics of Solids, 1977. **25**: p. 217-233.
31. Wang, Y.M., G.J. Weng, *Self-Similar and transient void growth in viscoelastic media at low concentrations.* International Journal of Fracture, 1993. **61**: p. 1-16.
32. Rice, J.R., D.M. Tracey, *On the ductile enlargement of voids in triaxial stress fields.* Journal of the Mechanics and Physics of Science, 1969. **17**: p. 201-217.
33. Tracey, *Strain-Hardening and Interaction Effects on the Growth of Voids in Ductile Fracture.* Engineering Fracture Mechanics, 1971. **3**: p. 301-315.
34. Tvergaard, V., *Influence of voids on shear band instabilities under plane strain conditions.* International Journal of Fracture, 1981. **17**(4): p. 389-407.
35. Tvergaard, V., *On localization in ductile materials containing spherical voids.* International Journal of Fracture, 1982. **18**(4): p. 237-252.
36. Hashin, Z., *Viscoelastic Behavior of Heterogeneous Media.* Journal of Applied Mechanics, 1965. **32**(3): p. 630-636.
37. Li, J.a.G.J.W., *Void growth in viscoelastic polymeric materials.* Mechanics of Plastics and Plastic Composites, ASME 1995, 1995. **68**: p. 409-421.
38. Li, J.a.G.J.W., *A unified approach from elasticity to viscoelasticity to viscoplasticity of particle reinforced solids.* International Journal of Plasticity, 1998. **14**(1-3): p. 293-208.
39. Clements, B.E., *Damage Evolution in Viscoelastic Polymers.* AIP Conference Proceedings, 1999. **505**(1): p. 527-530.
40. Steenbrink, A.C., E. Van Der Giessen, P.D. Wu, *Studies of the Growth of voids in amorphous glassy polymers.* Journal of Materials Science, 1998. **33**(12): p. 3163-3175.
41. Smit, R.J.M., W.A.M. Brekelmans, H.E.H. Meijer, *Predictive Modelling of the properties and toughness of polymeric materials: Part III: Macrostructural Deformation of rubber modified polymers.* Journal of Materials Science, 2000. **35**: p. 2881-2892.

42. McCrum, N.G., C,P. Buckley, C.B. Bucknall, *Principles of Polymer Engineering*. second ed. 1997, Oxford: Oxford University Press. 447.
43. Vigny, M., A. Aubert, J.M. Hiver, M. Aboulfaraj, C. G'Sell, *Constitutive Viscoplastic Behavior of Amorphous PET During Plant-Strain Tensile Stretching.* Polymer Engineering and Science, 1999. **39**(12): p. 2366-2376.
44. Bergstrom, J.S., and M. C. Boyce, *Constitutive Modeling of the Large Strain Time-Dependent Behavior of Elastomers.* Journal of the Mechanics and Physics of Science, 1998. **46**(5): p. 931-954.
45. Wu, J.D., and Kenneth M. Liechti, *Multiaxial and Time Dependent Behavior of a Filled Rubber.* Mechanics of Time-Dependent Materials, 2000(4): p. 293-331.
46. Sweeney, J., P. Caton-Rose, P.D. Coates, *The modelling of large deformations of pre-oriented polyethylene.* Polymer, 2001. **43**: p. 899-907.